

## Article

# Power Dissipation in the Subtectorial Space of the Mammalian Cochlea Is Modulated by Inner Hair Cell Stereocilia

Srdjan Prodanovic,<sup>1</sup> Sheryl Gracewski,<sup>1</sup> and Jong-Hoon Nam<sup>1,2,\*</sup><sup>1</sup>Department of Mechanical Engineering and <sup>2</sup>Department of Biomedical Engineering, University of Rochester, Rochester, New York

**ABSTRACT** The stereocilia bundle is the mechano-transduction apparatus of the inner ear. In the mammalian cochlea, the stereocilia bundles are situated in the subtectorial space (STS)—a micrometer-thick space between two flat surfaces vibrating relative to each other. Because microstructures vibrating in fluid are subject to high-viscous friction, previous studies considered the STS as the primary place of energy dissipation in the cochlea. Although there have been extensive studies on how metabolic energy is used to compensate the dissipation, much less attention has been paid to the mechanism of energy dissipation. Using a computational model, we investigated the power dissipation in the STS. The model simulates fluid flow around the inner hair cell (IHC) stereocilia bundle. The power dissipation in the STS because of the presence IHC stereocilia increased as the stimulating frequency decreased. Along the axis of the stimulating frequency, there were two asymptotic values of power dissipation. At high frequencies, the power dissipation was determined by the shear friction between the two flat surfaces of the STS. At low frequencies, the power dissipation was dominated by the viscous friction around the IHC stereocilia bundle—the IHC stereocilia increased the STS power dissipation by 50- to 100-fold. There exists a characteristic frequency for STS power dissipation,  $CF_{STS}$ , defined as the frequency where power dissipation drops to one-half of the low frequency value. The IHC stereocilia stiffness and the gap size between the IHC stereocilia and the tectorial membrane determine the characteristic frequency. In addition to the generally assumed shear flow, nonshear STS flow patterns were simulated. Different flow patterns have little effect on the  $CF_{STS}$ . When the mechano-transduction of the IHC was tuned near the vibrating frequency, the active motility of the IHC stereocilia bundle reduced the power dissipation in the STS.

## INTRODUCTION

Microstructures of the cochlear sensory-epithelium vibrate in a liquid-filled cavity. To explain the high-quality factor of hearing despite the power losses because of viscous friction, Gold predicted the existence of regenerative mechanisms in the cochlea (1). After decades of research, the outer hair cells were found to provide the regenerative force for the power amplification in the cochlea (2–4). The outer hair cells should operate optimally to provide enough power to compensate for the power loss because of viscous friction (5–9). The power gain in the cochlea has been estimated/measured to explain the operating principles of the cochlear amplifier (10–12). Although power amplification and outer hair cells' power output have both been investigated in many studies, the energy dissipation in the cochlea has rarely been studied (but see 13). To understand the power balance in the cochlea, it is necessary to understand not only where and how power is generated but also where and how power is dissipated as well.

Some types of hair cells, including the IHC in the mammalian cochlea, are stimulated by viscous forces because of fluid motion. There have been theoretical studies on how the fluid flow stimulates different hair cells (14–23).

Although the mechano-transduction of certain hair cells takes advantage of the viscous flow for the stimulation, the friction of the viscous flow also dissipates energy. For example, the IHC stereocilia bundle vibrates within a few micrometer-thin fluid layer in the STS. Fluid flow on such a small scale is highly viscous; it is inevitable for the hearing organ to undergo substantial viscous friction in the STS. Although most theoretical studies do not specify where/how acoustic energy is dissipated, there were suggestions on the source of cochlear energy dissipation, especially around the tectorial membrane. The viscoelasticity of the vibrating tissues in the cochlear partition such as the tectorial membrane have been considered as one mechanism of energy dissipation (24,25). A few studies considered the viscous friction in the STS as the primary cause of energy dissipation in the mammalian cochlea (26,27). The energy dissipation in the STS was estimated from the viscous friction of a Newtonian fluid between two parallel plates representing the tectorial membrane and the reticular lamina (7,8,27). However, the STS is more complex than a fluid layer between two parallel plates in shear motion because the IHCs' stereocilia may impede or interact with the flow. Moreover, there can be modes of vibrations different from shear motion in the STS (28–30).

The objective of this work is to investigate the power dissipation in the STS through numerical simulations. The model

Submitted June 9, 2014, and accepted for publication December 15, 2014.

\*Correspondence: [jong-hoon.nam@rochester.edu](mailto:jong-hoon.nam@rochester.edu)

Editor: Jochen Guck

© 2015 by the Biophysical Society  
0006-3495/15/02/0479/10 \$2.00



incorporates STS fluid dynamics, IHC stereocilia mechanics, and mechanical feedback because of transduction channel activation/adaptations. We explain the following: 1) how mechanical and geometric properties of the stereocilia bundle affect power dissipation in the STS; 2) how power dissipation in the STS changes under different stimulation modes; and 3) how force on the fluid generated by the IHC stereocilia bundle motility affects power dissipation in the STS.

## MATERIALS AND METHODS

Similar to previous studies (15,18,23) the STS is represented by a two-dimensional rectangular fluid domain containing a hinged, rigid rod representing the IHC stereocilia bundle (Fig. 1). The rod is located in the center of the domain and the rotational spring at the rod's base represents the stereocilia bundle stiffness. Whereas the STS length is fixed at  $L = 40 \mu\text{m}$ , two different IHC stereocilia bundle heights,  $h = 2$  and  $5 \mu\text{m}$ , are considered to roughly represent the basal and the apical locations, respectively (31–33). The height of the STS,  $H$ , is  $2.1 \mu\text{m}$  (basal) and  $5.25 \mu\text{m}$  (apical) with the standard gap size.

The top and the bottom boundaries represent the tectorial membrane and the reticular lamina, respectively. The bottom boundary is fixed so the top boundary motion represents the relative motion of the tectorial membrane with respect to the reticular lamina. The right boundary represents the stereocilia bundle of the second-row outer hair cells (middle one of the three outer hair cells in Fig. 1 A). It is hinged at the top and the bottom. The left boundary represents the opening toward the inner sulcus. No-slip boundary conditions are imposed along the top, bottom, and right boundary and along the IHC stereocilia bundle. The velocity boundary condition at the left boundary (the inner sulcus) is assigned so that the net flux through the boundaries of the simulated rectangular domain becomes zero.

Although we assumed specific dimensions, geometry, and mechanical properties of the IHC stereocilia bundle, they vary across different species

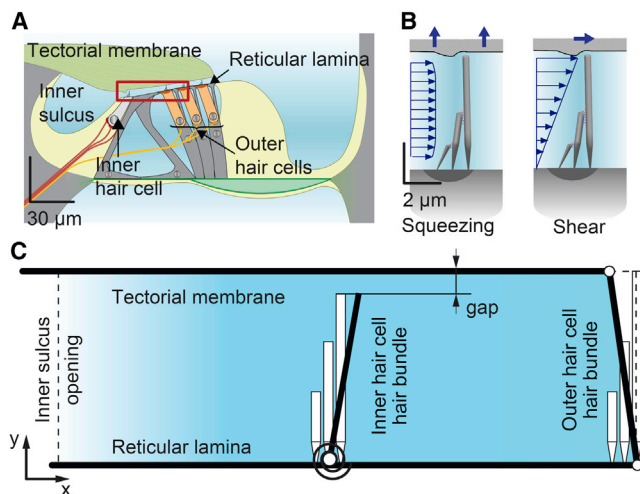


FIGURE 1 Fluid dynamics in the STS. (A) The organ of Corti. The red rectangle indicates the modeled part of STS. (B) Two different modes of STS motion resulting in squeezing and shear flow. (C) Model of the STS. The model consists of a rectangular fluid domain with boundaries representing the second-row outer hair cell stereocilia bundle, tectorial membrane, and reticular lamina, and a rigid rod hinged at the root representing the IHC stereocilia bundle. The torsional spring at the hinge represents the flexural rigidity of the IHC stereocilia. Hensen's stripe is not modeled (see Discussion). The displacements are exaggerated for illustrative purposes. To see this figure in color, go online.

and cochlear locations (32–37). The gap size between the tips of IHC stereocilia and the tectorial membrane is a key model parameter. The stiffness of the IHC stereocilia bundle was measured in several species such as Guinea pig (38), mouse (39), and rat (40). At the apical turn of the rat cochlea, the stiffness of the IHC stereocilia bundle was measured to be 2.5 to 3.5 mN/m (40). In recent studies, microprobes used to measure the bundle stiffness were found to affect hair cell mechano-transduction by unevenly deflecting the stereocilia bundle (41–44). This probe artifact should underestimate the bundle stiffness especially the IHC stereocilia bundle with a wall-like stereocilia arrangement (45). Considering the probe artifact, we used 10 mN/m for the stereocilia bundle stiffness at the apex. For the basal model, 100 mN/m was used after considering the height. Unlike the stereocilia bundle stiffness, there are no reported data about the gap size or geometry. Because these two model parameters (stiffness and gap size) were found to be important to STS fluid dynamics, we performed the parametric study for the properties that affect the STS power dissipation: IHC stereocilia stiffness and gap size between the tip of the IHC stereocilia bundle and the tectorial membrane. Finally, active mechano-transduction channels are added to the model to investigate the effect of active force feedback on the power dissipation in STS.

## Equations of fluid motion

The fluid is regarded as incompressible and the convective nonlinearities are negligible (15). The momentum and continuity equations are described in terms of fluid density ( $\rho$ ), viscosity ( $\mu$ ), pressure ( $P$ ), and velocity ( $v$ ) as in the following:

$$\rho \frac{\partial v}{\partial t} = -\nabla P + \mu \nabla^2 v, \quad (1)$$

$$\nabla \cdot v = 0. \quad (2)$$

Because the STS is subjected to cyclic stimulations, Eq. 1 and Eq. 2 can be rewritten in terms of angular frequency  $\omega$ :

$$i\omega\rho \hat{v}(x, y, \omega) = -\nabla \hat{P}(x, y, \omega) + \mu \nabla^2 \hat{v}(x, y, \omega), \quad (3)$$

$$\nabla \cdot \hat{v}(x, y, \omega) = 0, \quad (4)$$

where  $\hat{P}(x, y, \omega)$  and  $\hat{v}(x, y, \omega)$  represent complex amplitudes of the fluid pressure and velocity, respectively, and  $i$  is the imaginary unit.

## Combining active mechanics of the IHC stereocilia bundle and STS fluid dynamics

The displacement of the active IHC stereocilia bundle  $X$  is described by the following equation:

$$c_{HB} \frac{dX(t)}{dt} + k_{HB} X(t) = F(t) + F_{MT}(t), \quad (5)$$

where  $F(t)$  is the effective hydrodynamic force at the IHC stereocilia bundle tip,  $k_{HB}$  is the IHC stereocilia stiffness, and  $c_{HB}$  represents the internal viscous friction between the IHC stereocilia. The  $c_{HB}$  is expected to be small because of the minimal separating motion between stereocilia (46). The inertial force term due to stereocilia bundle mass was omitted because it is negligible compared with viscous or elastic force (see Supporting Material).  $F_{MT}$  is the active force exerted by the mechano-transduction channels (47) given as the following:

$$F_{MT}(t) = N \gamma k_G b p_O(t). \quad (6)$$

The force  $F_{MT}$  is determined by the open probability of mechano-transduction channels ( $p_o$ ), the gating spring stiffness ( $k_G$ ), the gating swing ( $b$ ), and the geometrical gain factor ( $\gamma$ ).

The active mechanism is represented by the ten-state channel kinetics model from previous work (48). The adaptation is mediated by  $\text{Ca}^{2+}$  entering through the mechano-transduction channels. The rate change of probability of the channel states ( $d\mathbf{p}/dt$ ) is described as a function of stereocilia bundle displacement,  $X$ :

$$\frac{d\mathbf{p}}{dt} = \mathbf{A}(X)\mathbf{p} + \mathbf{B}(X), \quad (7)$$

where  $\mathbf{A}$  is a  $9 \times 9$  coefficient matrix, and  $\mathbf{B}$  is a column vector. After linearization and by assuming small harmonic excitation about the resting position, Eq. 7 becomes the following:

$$\hat{\mathbf{p}}(\omega) = (i\omega \mathbf{I} - \mathbf{A}_0)^{-1}(\mathbf{A}'_0 \mathbf{p}_0 + \mathbf{B}'_0)\hat{X}(\omega), \quad (8)$$

where  $\hat{\mathbf{p}}(\omega)$  and  $\hat{X}(\omega)$  are the alternating components of  $\mathbf{p}$  and  $X$ , respectively, when stimulated at the angular frequency  $\omega$ . The variables with the subscript 0 indicate the properties evaluated at the equilibrium (resting) state.  $\mathbf{A}'_0$  and  $\mathbf{B}'_0$  are derivatives of  $\mathbf{A}$  and  $\mathbf{B}$  with respect to  $X$  at  $X_0$ , and  $\mathbf{I}$  is the identity matrix. Derivation procedures and detailed equations of the channel kinetics model are given in the [Supporting Material](#).

Considering harmonic oscillations with an angular frequency  $\omega$ , Eq. 5 becomes the following:

$$\hat{U}(\omega)(c_{HB} - i k_{HB}/\omega) = \hat{F}(\omega) + \hat{F}_{MT}(\omega), \quad (9)$$

where  $\hat{U}(\omega)$  is the alternating component of the velocity of the IHC stereocilia bundle tip. The effective hydrodynamic force  $\hat{F}(\omega)$  at the tip is obtained by dividing the total hydrodynamic torque on the IHC stereocilia bundle (integral of the pressure difference  $\Delta\hat{P}(\omega)$  across the IHC stereocilia bundle) by the bundle height  $h$ :

$$\hat{F} = \frac{1}{h} \int_0^h y \Delta\hat{P}(\omega) dy. \quad (10)$$

Hereafter, the hats will be dropped from the equations for simplicity.

## Computation

Discretization procedures and model parameters are given in the [Supporting Material](#). The overall problem size depends on the gap size between the IHC stereocilia bundle tip and the tectorial membrane because the mesh size has to be less than one-quarter of the gap size to resolve the flow pattern through the gap. The problem was solved on the BlueHive Cluster in the Center for Integrated Research Computing at the University of Rochester. It took between 0.5 to 5 h to solve for one frequency depending on the problem size.

## RESULTS

Geometric and mechanical parameters such as gap size between the IHC stereocilia bundle tip and the tectorial membrane, STS dimensions, and the IHC stereocilia stiffness determine the power dissipation in the STS. Because of the uncertainty of key model parameters such as the gap size and the IHC stereociliar stiffness, a series of parametric studies was performed. Even if we use the terms such as apical and basal model hereafter, it does not mean a specific location with well-defined characteristic frequency. They

rather refer to tall ( $5 \mu\text{m}$ ) or short ( $2 \mu\text{m}$ ) IHC stereocilia bundle (e.g., 31–33,49), respectively. Although we cannot be specific to which location/species the models correspond because of the lack of information about the STS geometry, the tall (apical) and the short (basal) model roughly represent low ( $\sim 1$  kHz) and high frequency ( $\sim 20$  kHz) locations of the mammalian cochlea, respectively. Therefore, the tall model was simulated for a frequency range between 0.1 and 10 kHz, and the short model between 1 and 100 kHz. At first, the mechano-transduction channels, the active force  $F_{MT}$  in Eq. 5, will not be included in the model. The effect of active force feedback is presented at the end of this section.

## Power dissipation in the STS

Power dissipation in the STS is evaluated as the rate of work done along the boundaries of STS. Conservation of energy for steady-state oscillation dictates that the rate of work done along the boundaries is equal to the power dissipated within the domain. The boundaries include the tectorial membrane, the outer hair cell's stereocilia bundle, and the inner sulcus. Work is not done on the reticular lamina boundary because it is stationary. The external force acting on the fluid at the boundary is equal to the internal force from the fluid acting on the boundaries. This force results from the normal and the shear stresses (50) as in the following:

$$\begin{cases} \sigma_{xx} = -P + 2\mu(\partial U/\partial x) \\ \sigma_{yy} = -P + 2\mu(\partial V/\partial y) \\ \tau_{xy} = \mu(\partial U/\partial y + \partial V/\partial x) \end{cases}, \quad (11)$$

where  $P$  is pressure, and  $U$  and  $V$  are horizontal and vertical fluid velocity components, respectively. The cycle averaged rate of work done at the outer hair cell boundary ( $P_{OHC}$ ), at the inner sulcus boundary ( $P_{IS}$ ), and at the tectorial membrane boundary ( $P_{TM}$ ) are obtained by integrating over the boundary the product of the boundary velocity and the resultant force of the stresses acting on the boundary:

$$P_{OHC} = \frac{1}{2} \text{Re} \left( - \int_0^H \sigma_{xx} U_{OHC}^* dy + \mu \int_0^H \tau_{xy} V_{OHC}^* dy \right), \quad (12)$$

$$P_{IS} = \frac{1}{2} \text{Re} \left( \int_0^H \sigma_{xx} U_{IS}^* dy - \mu \int_0^H \tau_{xy} V_{IS}^* dy \right), \quad (13)$$

$$P_{TM} = \frac{1}{2} \text{Re} \left( \mu \int_0^L \tau_{xy} U_{TM}^* dx - \int_0^L \sigma_{yy} V_{TM}^* dx \right). \quad (14)$$

The superscript asterisk indicates complex conjugate. The total power dissipated within the STS is the sum of  $P_{OHC}$ ,  $P_{TM}$  and  $P_{IS}$ , or  $P_{STS} = P_{OHC} + P_{TM} + P_{IS}$ . The result is obtained from the two-dimensional model, and it represents the power dissipation per unit depth (1  $\mu\text{m}$ ). The dissipated power is normalized by  $P_0$ , the power dissipation of the viscous shear flow between two parallel plates in terms of the plate length ( $L$ ) and the STS height ( $H$ ). See the [Supporting Material](#) for derivation.

$$P_0 = 0.5 \mu(L/H)U_0^2. \quad (15)$$

### Factors that affect power dissipation in the STS

The normalized dissipated power when the upper boundary moves with the velocity  $U = U_0 \cos(\omega t)$  is shown in [Fig. 2](#). The presence of the IHC stereocilia bundle increases the power dissipation in the STS ( $P_{STS}/P_0 > 1$ ). As the frequency  $\omega$  increases, the hydrodynamic force of the fluid dominates over elastic force of the IHC stereocilia stiffness and the normalized power dissipation asymptotically decreases to 1. As the frequency  $\omega$  decreases, the power dissipation increases to the level of dissipation that would occur if the IHC stereocilia bundle were a rigid wall. The transition between the two limiting power dissipation regimes occurs within the audible frequency range of mammals (0.1 to 100 kHz). The characteristic frequency of STS power dissipation,  $CF_{STS}$  is defined as the frequency where the power dissipation drops to one-half of the maximum value, or the phase difference between the hair bundle and the tectorial membrane becomes 45 degrees. The  $CF_{STS}$  is 0.5 and 2.8 kHz in the apical model with the gap sizes 0.5 and 1.25  $\mu\text{m}$ , respectively (indicated by solid square markers). For the basal model, the  $CF_{STS}$  is 1.5 and 28 kHz when the gap sizes are 0.1 and 0.5  $\mu\text{m}$ , respectively. When the gap size is very small (0.1 and 0.05  $\mu\text{m}$  for the apical and the basal models, respectively), the  $CF_{STS}$  is lower than the lowest simulated frequency (0.1 and 1 kHz for the apical and the basal models, respectively).

Two main parameters determining the  $CF_{STS}$  and the power dissipation are the gap size and the stiffness of the IHC stereocilia bundle. As [Fig. 2](#) shows, the gap size between the tip of the IHC stereocilia bundle and the tectorial membrane strongly affects the power dissipation. For 1 kHz stimulation to the apical model, as the gap size changes from 1.25 to 0.5 and 0.1  $\mu\text{m}$ , the normalized power dissipation changes non-monotonically from 8 to 12 and 2 ([Fig. 2 A](#)). For 20 kHz stimulation to the basal model, as the gap size decreases from 0.5 to 0.1 and 0.05  $\mu\text{m}$ , the normalized power dissipation changes monotonically from 3 to 1.5 and 1.2 ([Fig. 2 B](#)). To further investigate the relations between the power dissipation and the gap size and the IHC stereocilia stiffness, the apical model was stimulated with different stiffness and gap size values in the frequency range from 0.1 to 10 kHz

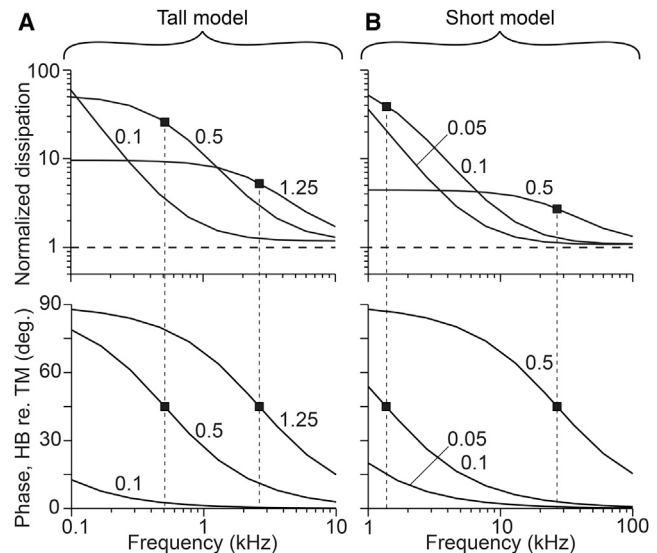


**FIGURE 2** Power dissipation in the STS and  $CF_{STS}$ . (A) Tall (apical) model. (B) Short (basal) model. Top panels: Normalized power dissipation. Bottom panels: Phase of the hair bundle with respect to the tectorial membrane. Labels on the curves indicate the size of the gap between the IHC stereocilia bundle tip and the tectorial membrane (in  $\mu\text{m}$ ). Stereocilia bundle stiffness is 10 and 100 mN/m for the tall and short models, respectively. The broken horizontal lines represent power obtained from the same model without the IHC stereocilia bundle ( $P_0$ ). The broken vertical lines indicate  $CF_{STS}$ , which correspond to half power dissipation or 45 degrees of phase difference.

([Fig. 3](#)). The normalized power dissipation increases with the stereocilia bundle stiffness, reaching the maximum value of  $\sim 200$  ([Fig. 3 A](#)). As a reference, the response that we believe reasonable (standard values: the stereocilia bundle stiffness of 10 mN/m, the best responding frequency of the location of 1 kHz, and the gap size of 0.25  $\mu\text{m}$ ) was indicated with circles in [Fig. 3, B–D](#). In the vicinity of the standard values, as the gap size increased, more power was dissipated near the assumed operating frequency (1 kHz), but at lower frequencies ( $< 1$  kHz) there exists a gap size that maximized the power dissipation ([Fig. 3 B](#)). As the stereocilia bundle stiffness increased, more power was dissipated ([Fig. 3 C](#)). Near the standard parameter values, smaller gap size and stereocilia bundle stiffness resulted in less power dissipation ([Fig. 3 D](#)). The basal model shows similar trend as the apical region (see the [Supporting Material](#)).

Since ter Kuile's kinematical analysis (51), it has been widely accepted that the IHC stereocilia bundle is stimulated by shear flow (26,37,52). However, the existence of nonshear flow in the STS has been suggested by several recent studies (28–30). We simulated nonshear stimulation modes, called squeezing modes in this work. Two simplistic squeezing modes were considered ([Fig. 4, A and B](#)). The first squeezing mode, [Fig. 4 A](#), represents the fundamental transverse vibrating mode of the tectorial membrane. The second squeezing mode, [Fig. 4 B](#), corresponds to a higher vibrating

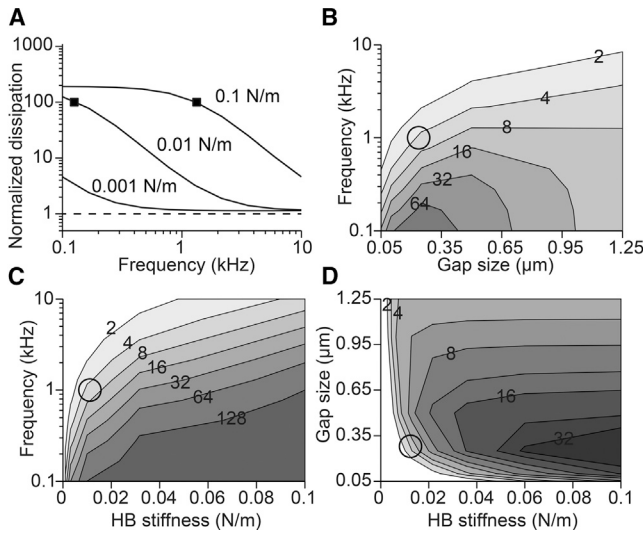


FIGURE 3 Effect of stereocilia bundle stiffness and gap size on STS power dissipation (Tall model). (A) Normalized power dissipation as function of frequency for three different values of the IHC stereocilia bundle stiffness; the gap size is  $0.25 \mu\text{m}$ . Solid square symbols indicate  $CF_{\text{STS}}$ . Contour plots of normalized power dissipation. (B) Effect of the gap size and the stimulating frequency; stiffness is  $10 \text{ mN/m}$ . (C) Effect of the stereocilia bundle stiffness and the stimulating frequency; the gap size is  $0.25 \mu\text{m}$ . (D) Effect of the stereocilia bundle stiffness and the gap size; the stimulating frequency is  $1 \text{ kHz}$ . The circles (B–D) indicate the standard parameter values of the apical model (see text). The base model result is shown in Fig. S4.

mode, and it has a zero velocity node above the IHC stereocilia bundle. Although there are reports that the outer hair cell stereocilia can elongate or shrink (53), in our study, outer hair cell stereocilia length remains unchanged.

The power dissipation of the squeezing modes is greater than that of the shear mode, although the difference is not considerable. Three modes are compared through their corresponding normalized power dissipation (Fig. 4 D). Although the motion of the tectorial membrane is distinct for each mode, the flow patterns near the IHC stereocilia are similar (Fig. 4, A–C). This similarity in flow pattern, because of the same boundary conditions at the stereocilia, may explain why the frequency-power dissipation curves are similar despite different stimulating modes (Fig. 4, D and E). Although we did not see a substantial difference in power dissipation and the  $CF_{\text{STS}}$  is nearly the same, we are hesitant to conclude that different stimulating modes have the same effect on the IHC mechano-transduction. How different modes affect the mechano-transduction may need further investigation considering the organ of Corti vibrations (8,28–30,54), but it is beyond the scope of this study.

### Can the force feedback from IHC mechano-transduction affect the STS power dissipation?

So far all the results are obtained with the stereocilia bundle without incorporating active force feedback from the me-

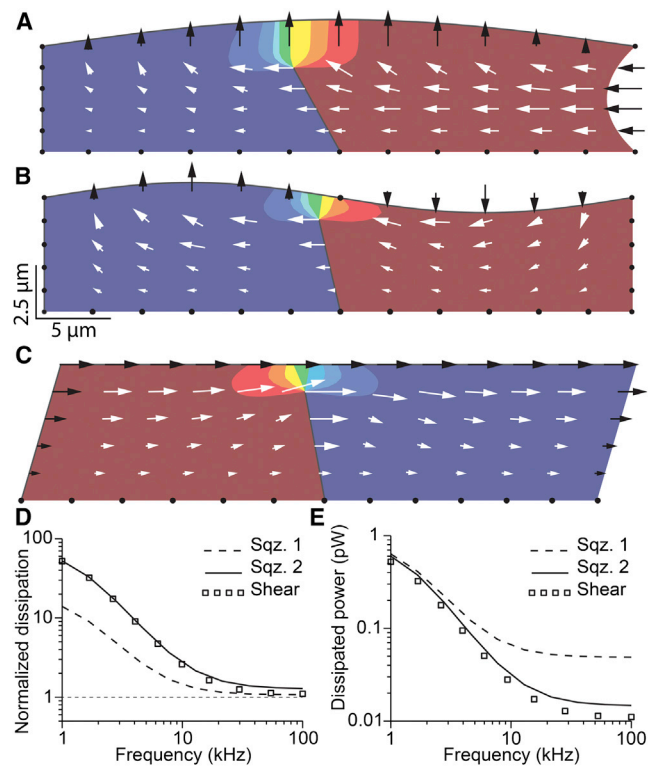


FIGURE 4 Effect of different stimulation modes (short model). Snapshots of pressure (hotter color indicates higher pressure) and velocity (arrows) fields from (A) the first squeezing mode, (B) the second squeezing mode, and (C) the shear mode. (D) Normalized power dissipation from all three modes. The squeezing modes' power dissipation is normalized by the dissipation from the same model, but without the IHC stereocilia bundle. (E) Comparison of the absolute dissipated power from the three modes. Boundary velocities were chosen so the volumetric flux through the IHC stereocilia bundle plane is constant. To see this figure in color, go online.

chano-transduction channels in the IHC stereocilia. According to measurements from nonmammalian and mammalian hair cells (e.g., 55–57), a single hair cell bundle can generate force of the order of  $100 \text{ pN}$ . Although there is no direct measurement of IHC's active force, there are measurements showing the adaptation of IHC's mechano-transduction and nonlinear mechanics (39,40,58) similar to other types of hair cells. The adaptation is considered to reflect the active mechanical feedback from the stereocilia (59,60). We investigated whether the active feedback of IHC stereocilia bundle can affect the power dissipation in the STS.

The active force of the stereocilia in our model (Eq. 6) follows conventional gating theory (47). Previous studies showed that auditory hair cells can be highly tuned at certain frequencies (48,61). Stereocilia bundle parameters were chosen within the physiologically relevant range to obtain a tuned response of the stereocilia bundle. While all other model parameters remained the same, different levels of the mechano-transduction force (different gating swings) were tested to adjust the level of tuning. First, the response

of mechano-transduction was simulated without fluid interaction; an isolated active stereocilia bundle from the tall and the short models was stimulated by a sinusoidal force (Fig. 5, A and C). As the gating swing changes from 2.9 to 2.7 and 2.0 nm, the stereocilia bundle's frequency responses change from highly-tuned to moderately-tuned and untuned.

After testing isolated bundles, the full model with fluid interaction was simulated. Active stereocilia bundle reduced the STS power dissipation, for the tall (Fig. 5 B) and the short (Fig. 5 D) models. When the stereocilia bundle is highly tuned because of active mechanical feedback from the mechano-transduction channels, the stereocilia bundle provides power to the STS rather than dissipates power: negative power dissipation around 0.55 and 3 kHz for the tall and the short models, respectively (thick solid line in Fig. 5, B and D). Moderately and poorly tuned stereocilia bundle also reduced power dissipation compared with the passive bundle.

A stereocilia bundle, tuned by active mechano-transduction channels, can provide power to the surrounding fluid. The phase relation between bundle velocity and the force the bundle exerts on the surrounding fluid explains modulation of the power dissipation in the STS by the active stereocilia bundle. The force exerted on the fluid is equal to and opposite of the force  $F$  in Eq. 5. When the STS with a highly tuned stereocilia bundle is stimulated at the tuned frequency (0.55 or 3 kHz), the force is almost in phase with the veloc-

ity and the bundle provides power per cycle to the surrounding fluid (Fig. 6 A). If the stereocilia bundle is poorly tuned, or highly tuned bundle is stimulated away from its tuned frequency (at 0.1 kHz), the force leads the velocity by a half cycle and the bundle dissipates power per cycle (Fig. 6, B–C). For the moderately tuned bundle stimulated at its tuned frequency (0.9 kHz), the force leads the velocity by a quarter cycle, and the bundle neither provides nor dissipates power (Fig. 6 D). In conclusion, properly tuned stereocilia bundle, stimulated at its tuned frequency, can greatly reduce power dissipation in the STS. A movie in the Supporting Material demonstrates the cases of Fig. 6, A and B.

## DISCUSSION

### Characteristic frequency of STS power dissipation: $CF_{STS}$

Our results show that there are two dynamic regimes of fluid-structure interaction in the STS. At high frequencies, the IHC stereocilia bundle does not impede fluid flow so that the power dissipation in the STS asymptotes to the value expected from simple viscous friction between two parallel plates. At low frequencies, the IHC stereocilia bundle is hardly deflected by the fluid flow. The stereocilia bundle behaves like a rigid wall, increasing the power dissipation by more than two orders of magnitude compared with the high-frequency case (Fig. 2, when the gap size is  $\leq 0.1 \mu\text{m}$ ). Interestingly,  $CF_{STS}$ , the frequency defining the transition point between these two regimes, is in a physiologically meaningful frequency range (between 0.1 and 100 kHz, Fig. 2) as long as the gap size is greater than 5% of the stereocilia bundle height.

The characteristic frequency of STS power dissipation,  $CF_{STS}$ , is determined by the balance between two forces—the viscous drag and the elastic restoring force of the IHC stereocilia bundle. As the bundle stiffness increases, the elastic restoring force becomes dominant so that the stereocilia bundle acts like a rigid wall impeding the fluid flow. As a result, the  $CF_{STS}$  shifts to higher value (Fig. 3 A). As the gap size decreases, the drag force experienced by the stereocilia bundle increases compared with elastic restoring force. The  $CF_{STS}$  shifts to the left along the frequency axis (Fig. 2).

### A possible role of active force from the IHC stereocilia

Our work suggests two possible ways that the mammalian hearing organ can benefit from the power dissipation because of the IHC stereocilia bundle. First, the cochlea can take advantage of a passive mechanism. Using a physiologically realistic IHC stereocilia bundle stiffness and gap size, we showed that the  $CF_{STS}$  falls within the hearing range of mammals (Fig. 2). If the  $CF_{STS}$  is near the best responding frequency of the location of the IHC, the

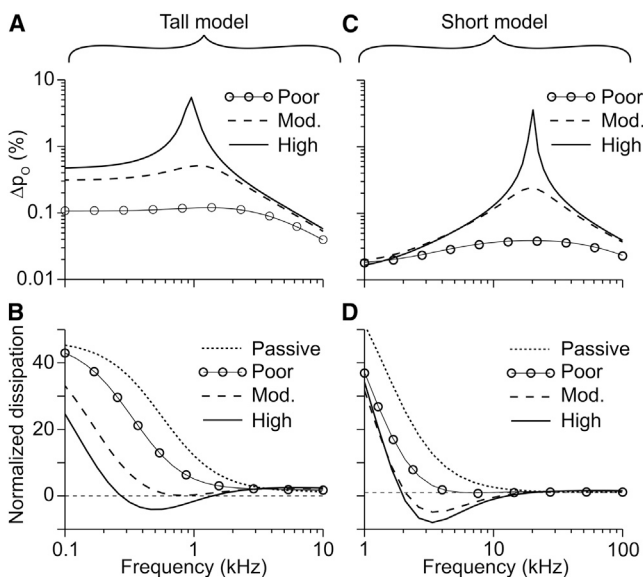


FIGURE 5 Active IHC stereocilia modulate STS power dissipation. (A) Normalized IHC transduction current ( $\Delta p_0$ ) of the tall model. (B) Normalized STS power dissipation of the tall model. (C) Normalized IHC transduction current of the short model. (D) Normalized STS power dissipation of the short model. Gap size and bundle stiffness are 0.5 and 0.1  $\mu\text{m}$  and 10 and 100 mN/m, for the tall and the short models, respectively. Results in (A) and (B) are without fluid-interaction. Four cases were simulated: three different tuning levels of the active IHC and the passive IHC.

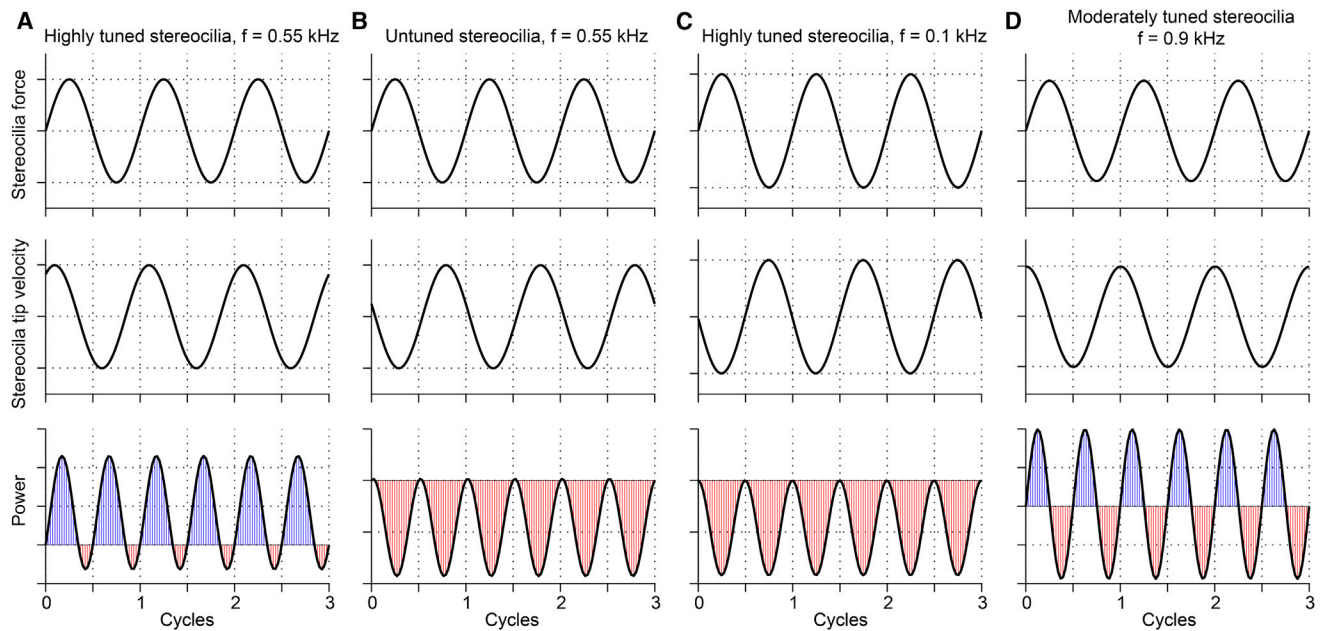


FIGURE 6 Power dissipation is determined by phase relation. (A) Highly tuned IHC stereocilia bundle ( $Q_{3dB} = 16$ ); stimulating frequency is 0.55 kHz. (B) Untuned transduction IHC stereocilia bundle; stimulating frequency is 0.55 kHz. (C) Highly tuned IHC stereocilia bundle ( $Q_{3dB} = 16$ ); stimulating frequency is 0.1 kHz. (D) Moderately tuned ( $Q_{3dB} = 1.6$ ) IHC stereocilia bundle, stimulating frequency is 0.9 kHz. Top row in all panels: force exerted by the stereocilia bundle on the surrounding fluid. Middle row in all panels: velocity of the stereocilia tip. Blue color indicates power transmitted to the fluid from the stereocilia bundle; red color indicates dissipated power (shaded area above and below the horizontal line, respectively). To see this figure in color, go online.

additional power dissipation because of the IHC stereocilia can sharpen the frequency tuning by acting as a high-pass filter. This idea of the IHC stereocilia bundle as a high-pass filter is in agreement with previous studies (14,17,19). Secondly, the mammalian cochlea can use the active mechanism of the IHC stereocilia bundle to modulate power dissipation. It is known that the bundle has at least two active adaptation mechanisms distinguished by their operating speeds (41,62,63). It has been measured/estimated that a single stereocilia bundle can generate at least tens of pN of force (40,47,55,64). Although the active stereocilia bundle mechanics of IHC is less investigated compared with nonhearing hair cells or outer hair cells, the adaptation of mechano-transduction current (e.g., 65) and the dependence of stereocilia bundle mechanics on mechano-transduction (39,40) indicate that the IHC stereocilia can also generate forces similar to other types of hair cells. In this study, the single-channel gating force (the product of the gating swing and gating spring stiffness), the force generated by a single channel because of its configuration change (47), ranges between 7 and 12 pN, which is comparable with the values in other studies with mammalian cochlear hair cell (48,66). After considering the number of channels and the geometrical gain, this single-channel gating force corresponds to  $\sim 100$  and 250 pN per stereocilia bundle of the tall and the short models, respectively.

When the active force is applied with proper timing (phase) with respect to the external stimulation, our results (Figs. 5 and 6) show that the IHC stereocilia bundle provides

energy instead of dissipating it. This seems surprising in that a stereocilia bundle can overcome arguably primary energy dissipation (26,27) in the cochlea. But, it is reasonable considering that the STS viscous friction is comparable with the viscous friction that a stereocilia bundle is subjected to in a hemi-infinite fluid space (48). For example, the friction coefficient of the STS (without the IHC stereocilia bundle) is  $\sim 50$  nNs/m ( $\mu Lb/H$ , where  $b$  is the width of a hair cell). This is comparable with the viscous friction experienced by a sphere with  $d = 8 \mu\text{m}$  ( $3\pi\mu d$ ). It was shown that the bullfrog sacculus stereocilia bundle overcomes the viscous drag over 100 nNs/m to oscillate spontaneously, and the actuator is considered the mechano-transduction channels in the stereocilia bundle (67).

Despite our simulated result of negative damping in the STS because of stereocilia bundle's feedback force, we do not argue that this instability exists in the cochlea. Our purpose was to explore physiologically possible range of stereocilia bundle's mechanical feedback. A conservative conclusion of our result is that the IHC stereocilia bundle (despite its tuning) can actively modulate the power dissipation in the STS through its mechanical feedback originating from its mechano-transduction channels. The modulation is more effective when the bundle operates near its unstable state (68).

### Inner hair cell tuning

The tuned IHC mechano-transduction in Fig. 5 is reminiscent of the nearly obsolete concept of a second filter (but,

see 69). A second filter in the cochlea implies any mechanism that is responsible for the difference between the mechanical tuning measured at the basilar membrane and the neural tuning of auditory nerve fibers (70). This concept has lost favor as the sharpness of the neural tuning and the mechanical tuning were found to be comparable (71). Our work was not intended to revisit the idea of a second filter because our analyses were limited to a subdomain of the entire cochlear mechanics. That said, it was shown that a small change in the channel kinetics can change the power dissipation in the STS dramatically (Fig. 5) by adjusting the phase of the active force from the stereocilia bundle with respect to the fluid flow (Fig. 6). In other words, the IHC stereocilia bundle acting as an active damper has a potential to affect overall cochlear mechanics.

There are two conditions under which the IHC can contribute to cochlear tuning through its modulation of power dissipation. First, the IHC can contribute to the mechanical tuning of the cochlear partition (the first filter) provided that this STS power dissipation dominates the overall power dissipation in the cochlear partition. Second, if the tectorial membrane vibrates independent of the basilar membrane (72,73), the IHC's modulation of STS power dissipation may contribute to a second filter through the mechanism suggested by Zwislocki (72).

The extent and magnitude of the power modulation by the IHC stereocilia bundle are determined by two factors—the force and the timing. In our work, the single-channel gating force determined the magnitude of the active force generated in the IHC stereocilia. The single-channel gating force is linearly proportional to the gating swing (47). By simulating different gating swing values, we showed the effect of the stereocilia bundle motility (Fig. 5). The timing (phase) of the active force application with respect to the fluid flow is determined by the characteristic frequency of stereocilia bundle. Fig. 6 demonstrates the effect of this timing. There are different theories on how the characteristic frequency of the hair cell mechano-transduction is determined (e.g., 48,66,74). The characteristic frequency in our model is determined by the adaptation speed, the activation speed of the mechano-transduction channel and the stereocilia bundle stiffness. Although a specific mechano-transduction model was used, our finding holds despite different mechano-transduction theories provided that an appropriate stereocilia bundle force (Fig. 5) is applied with the right timing (Fig. 6).

It is unclear whether the IHC's mechano-transduction is in phase with the basilar membrane displacement or velocity. Available data indicate that the phase relationship depends on the stimulation level and the stimulation frequency (75–78). Our results show that the IHC stereocilia bundle displacement is in phase with the STS shear displacement at high frequencies, but with STS shear velocity at low frequencies (Fig. 2). The frequency-dependence varies according to the bundle's mechanical feedback

(Figs. 5 and 6). For a better comparison with experimental results, however, the STS fluid dynamics should be solved in the context of whole organ of Corti mechanics.

### Limitations of this study—the importance of STS anatomy

Although there are available data regarding the IHC stereocilia bundle stiffness (39,58), there is very limited information about how the gap between the tips of the IHC stereocilia and the tectorial membrane is shaped. In particular, there is a characteristic ridge on the undersurface of the tectorial membrane, in the vicinity of the IHC stereocilia tips, known as the Hensen's stripe (79). The size, position, and connectivity to the IHC stereocilia bundle and reticular lamina are not well characterized. For example, whether Hensen's stripe is connected to the IHC stereocilia is unclear (35,80). In mice, the Hensen's stripe was not observed in apical (low frequency) locations of the cochlea as it was in basal locations (81).

Steele and his colleagues considered that the mechanical role of the Hensen's stripe is to provide a strong viscous coupling between the tectorial membrane and the IHC stereocilia (82,83). In their work, the computational cost of fluid dynamical analysis in the STS was reduced by deriving the viscous coupling term assuming Poiseuille flow between a plate (Hensen's stripe) and a cylinder (stereocilia tips). Although we did not include the Hensen's stripe because of anatomical uncertainty and computational complexity, based on Steele et al.'s work, we can presume its effect. If the Hensen's stripe has a significant depth and is close enough to the IHC stereocilia (comparable with the gap size), it will increase the viscous coupling between the tectorial membrane and the IHC stereocilia similar to the decrease in the gap size in our work.

### SUPPORTING MATERIAL

Supporting Material, four figures, one table, and two movies are available at [http://www.biophysj.org/biophysj/supplemental/S0006-3495\(14\)04774-2](http://www.biophysj.org/biophysj/supplemental/S0006-3495(14)04774-2).

### ACKNOWLEDGMENTS

This work was supported by NSF CMMI-1233595 and the University of Rochester via an HSCCI award.

### REFERENCES

1. Gold, T. 1948. Hearing. 2. The physical basis of the action of the cochlea. *Proc. R. Soc. Ser. B-Bio. Sci.* 135:492–498.
2. Brownell, W. E., C. R. Bader, ..., Y. de Ribaupierre. 1985. Evoked mechanical responses of isolated cochlear outer hair cells. *Science*. 227:194–196.
3. Ashmore, J. 2008. Cochlear outer hair cell motility. *Physiol. Rev.* 88:173–210.
4. Dallos, P. 2008. Cochlear amplification, outer hair cells and prestin. *Curr. Opin. Neurobiol.* 18:370–376.

5. Ospeck, M., X. X. Dong, and K. H. Iwasa. 2003. Limiting frequency of the cochlear amplifier based on electromotility of outer hair cells. *Biophys. J.* 84:739–749.
6. Rabbitt, R. D., S. Clifford, ..., W. E. Brownell. 2009. Power efficiency of outer hair cell somatic electromotility. *PLoS Comput. Biol.* 5:e1000444.
7. Sul, B., and K. H. Iwasa. 2009. Amplifying effect of a release mechanism for fast adaptation in the hair bundle. *J. Acoust. Soc. Am.* 126:4–6.
8. Nam, J. H., and R. Fettiplace. 2012. Optimal electrical properties of outer hair cells ensure cochlear amplification. *PLoS ONE.* 7:e50572.
9. Ramamoorthy, S., and A. L. Nuttall. 2012. Outer hair cell somatic electromotility in vivo and power transfer to the organ of Corti. *Biophys. J.* 102:388–398.
10. Shera, C. A. 2007. Laser amplification with a twist: traveling-wave propagation and gain functions from throughout the cochlea. *J. Acoust. Soc. Am.* 122:2738–2758.
11. Fisher, J. A. N., F. Nin, ..., A. J. Hudspeth. 2012. The spatial pattern of cochlear amplification. *Neuron.* 76:989–997.
12. Dong, W., and E. S. Olson. 2013. Detection of cochlear amplification and its activation. *Biophys. J.* 105:1067–1078.
13. Dong, W., and E. S. Olson. 2009. In vivo impedance of the gerbil cochlear partition at auditory frequencies. *Biophys. J.* 97:1233–1243.
14. Weiss, T. F., and R. Leong. 1985. A model for signal transmission in an ear having hair cells with free-standing stereocilia. III. Micromechanical stage. *Hear. Res.* 20:157–174.
15. Freeman, D. M., and T. F. Weiss. 1990. Superposition of hydrodynamic forces on a hair bundle. *Hear. Res.* 48:1–15.
16. Freeman, D. M., and T. F. Weiss. 1990. Hydrodynamic forces on hair bundles at low frequencies. *Hear. Res.* 48:17–30.
17. Freeman, D. M., and T. F. Weiss. 1990. Hydrodynamic forces on hair bundles at high frequencies. *Hear. Res.* 48:31–36.
18. Freeman, D. M., and T. F. Weiss. 1988. The role of fluid inertia in mechanical stimulation of hair cells. *Hear. Res.* 35:201–207.
19. Zetes, D. E., and C. R. Steele. 1997. Fluid-structure interaction of the stereocilia bundle in relation to mechanotransduction. *J. Acoust. Soc. Am.* 101:3593–3601.
20. Nam, J. H., J. R. Cotton, and J. W. Grant. 2005. Effect of fluid forcing on vestibular hair bundles. *J. Vestib. Res.* 15:263–278.
21. Shatz, L. F. 2004. The effect of hair bundle shape on hair bundle hydrodynamics of non-mammalian inner ear hair cells for the full frequency range. *Hear. Res.* 195:41–53.
22. Shatz, L. F. 2000. The effect of hair bundle shape on hair bundle hydrodynamics of inner ear hair cells at low and high frequencies. *Hear. Res.* 141:39–50.
23. Billone, M., and S. Raynor. 1973. Transmission of radial shear forces to cochlear hair cells. *J. Acoust. Soc. Am.* 54:1143–1156.
24. Sellon, J. B., R. Ghaffari, ..., D. M. Freeman. 2014. Porosity controls spread of excitation in tectorial membrane traveling waves. *Biophys. J.* 106:1406–1413.
25. Jones, G. P., V. A. Lukashkina, ..., A. N. Lukashkin. 2013. Frequency-dependent properties of the tectorial membrane facilitate energy transmission and amplification in the cochlea. *Biophys. J.* 104:1357–1366.
26. Allen, J. B. 1980. Cochlear micromechanics—a physical model of transduction. *J. Acoust. Soc. Am.* 68:1660–1670.
27. Mammano, F., and R. Nobili. 1993. Biophysics of the cochlea: linear approximation. *J. Acoust. Soc. Am.* 93:3320–3332.
28. Guinan, Jr., J. J. 2012. How are inner hair cells stimulated? Evidence for multiple mechanical drives. *Hear. Res.* 292:35–50.
29. Nowotny, M., and A. W. Gummer. 2006. Nanomechanics of the subtectorial space caused by electromechanics of cochlear outer hair cells. *Proc. Natl. Acad. Sci. USA.* 103:2120–2125.
30. Nowotny, M., and A. W. Gummer. 2011. Vibration responses of the organ of Corti and the tectorial membrane to electrical stimulation. *J. Acoust. Soc. Am.* 130:3852–3872.
31. Furness, D. N., S. Mahendrasingam, ..., C. M. Hackney. 2008. The dimensions and composition of stereociliary rootlets in mammalian cochlear hair cells: comparison between high- and low-frequency cells and evidence for a connection to the lateral membrane. *J. Neurosci.* 28:6342–6353.
32. Lim, D. J. 1980. Cochlear anatomy related to cochlear micromechanics. A review. *J. Acoust. Soc. Am.* 67:1686–1695.
33. Yarin, Y. M., A. N. Lukashkin, ..., T. Zahnert. 2014. Tonotopic morphometry of the lamina reticularis of the guinea pig cochlea with associated microstructures and related mechanical implications. *J. Assoc. Res. Otolaryngol.* 15:1–11.
34. Lim, D. J. 1986. Functional structure of the organ of Corti: a review. *Hear. Res.* 22:117–146.
35. Rueda, J., R. Cantos, and D. J. Lim. 1996. Tectorial membrane-organ of Corti relationship during cochlear development. *Anat. Embryol. (Berl.)*. 194:501–514.
36. Edge, R. M., B. N. Evans, ..., P. Dallos. 1998. Morphology of the unfixed cochlea. *Hear. Res.* 124:1–16.
37. Dallos, P. 2003. Organ of Corti kinematics. *J. Assoc. Res. Otolaryngol.* 4:416–421.
38. Strelieff, D., and A. Flock. 1984. Stiffness of sensory-cell hair bundles in the isolated guinea pig cochlea. *Hear. Res.* 15:19–28.
39. Russell, I. J., M. Kössl, and G. P. Richardson. 1992. Nonlinear mechanical responses of mouse cochlear hair bundles. *Proc. Biol. Sci.* 250:217–227.
40. Beurg, M., J. H. Nam, ..., R. Fettiplace. 2008. The actions of calcium on hair bundle mechanics in mammalian cochlear hair cells. *Biophys. J.* 94:2639–2653.
41. Peng, A. W., T. Effertz, and A. J. Ricci. 2013. Adaptation of mammalian auditory hair cell mechanotransduction is independent of calcium entry. *Neuron.* 80:960–972.
42. Karavitaki, K. D., and D. Corey. 2014. A new probe for cochlear hair bundle stimulation. In Association for Research in Otolaryngology Midwinter Meeting, San Diego, CA.
43. Indzhukulian, A. A., R. Stepanyan, ..., G. I. Frolenkov. 2013. Molecular remodeling of tip links underlies mechanosensory regeneration in auditory hair cells. *PLoS Biol.* 11:e1001583.
44. Corns, L. F., S. L. Johnson, ..., W. Marcotti. 2014. Calcium entry into stereocilia drives adaptation of the mechano-electrical transducer current of mammalian cochlear hair cells. *Proc. Natl. Acad. Sci. USA.* 111:14918–14923.
45. Langer, M. G., S. Fink, ..., J. P. Ruppertsberg. 2001. Lateral mechanical coupling of stereocilia in cochlear hair bundles. *Biophys. J.* 80:2608–2621.
46. Kozlov, A. S., J. Baumgart, ..., A. J. Hudspeth. 2011. Forces between clustered stereocilia minimize friction in the ear on a subnanometre scale. *Nature.* 474:376–379.
47. Howard, J., and A. J. Hudspeth. 1988. Compliance of the hair bundle associated with gating of mechano-electrical transduction channels in the bullfrog's saccular hair cell. *Neuron.* 1:189–199.
48. Nam, J. H., and R. Fettiplace. 2008. Theoretical conditions for high-frequency hair bundle oscillations in auditory hair cells. *Biophys. J.* 95:4948–4962.
49. Nadol, Jr., J. B. 1988. Comparative anatomy of the cochlea and auditory nerve in mammals. *Hear. Res.* 34:253–266.
50. Batchelor, G. K. 1967. An Introduction to Fluid Dynamics. Cambridge University Press, Cambridge, UK.
51. ter Kuile, E. 1900. Die Übertragung der Energie von der Grundmembran auf die Haarzellen. *Pflügers Archiv. European J. Physiol.* 79:146–157.
52. Rhode, W. S., and C. D. Geisler. 1967. Model of the displacement between opposing points on the tectorial membrane and reticular lamina. *J. Acoust. Soc. Am.* 42:185–190.
53. Hakizimana, P., W. E. Brownell, ..., A. Fridberger. 2012. Sound-induced length changes in outer hair cell stereocilia. *Nat. Commun.* 3:1094.

54. Nam, J. H. 2014. Microstructures in the organ of Corti help outer hair cells form traveling waves along the cochlear coil. *Biophys. J.* 106:2426–2433.
55. Kennedy, H. J., A. C. Crawford, and R. Fettiplace. 2005. Force generation by mammalian hair bundles supports a role in cochlear amplification. *Nature.* 433:880–883.
56. Ricci, A. J., A. C. Crawford, and R. Fettiplace. 2002. Mechanisms of active hair bundle motion in auditory hair cells. *J. Neurosci.* 22:44–52.
57. Bozovic, D., and A. J. Hudspeth. 2003. Hair-bundle movements elicited by transepithelial electrical stimulation of hair cells in the sacculus of the bullfrog. *Proc. Natl. Acad. Sci. USA.* 100:958–963.
58. Beurg, M., M. G. Evans, ..., R. Fettiplace. 2006. A large-conductance calcium-selective mechanotransducer channel in mammalian cochlear hair cells. *J. Neurosci.* 26:10992–11000.
59. Assad, J. A., and D. P. Corey. 1992. An active motor model for adaptation by vertebrate hair cells. *J. Neurosci.* 12:3291–3309.
60. Ricci, A. J., A. C. Crawford, and R. Fettiplace. 2000. Active hair bundle motion linked to fast transducer adaptation in auditory hair cells. *J. Neurosci.* 20:7131–7142.
61. Choe, Y., M. O. Magnasco, and A. J. Hudspeth. 1998. A model for amplification of hair-bundle motion by cyclical binding of Ca<sup>2+</sup> to mechano-electrical-transduction channels. *Proc. Natl. Acad. Sci. USA.* 95:15321–15326.
62. Eatock, R. A. 2000. Adaptation in hair cells. *Annu. Rev. Neurosci.* 23:285–314.
63. Fettiplace, R., and A. J. Ricci. 2003. Adaptation in auditory hair cells. *Curr. Opin. Neurobiol.* 13:446–451.
64. Jaramillo, F., and A. J. Hudspeth. 1993. Displacement-clamp measurement of the forces exerted by gating springs in the hair bundle. *Proc. Natl. Acad. Sci. USA.* 90:1330–1334.
65. Kros, C. J., A. Rüscher, and G. P. Richardson. 1992. Mechano-electrical transducer currents in hair cells of the cultured neonatal mouse cochlea. *Proc. Biol. Sci.* 249:185–193.
66. Tinevez, J. Y., F. Jülicher, and P. Martin. 2007. Unifying the various incarnations of active hair-bundle motility by the vertebrate hair cell. *Biophys. J.* 93:4053–4067.
67. Martin, P., and A. J. Hudspeth. 1999. Active hair-bundle movements can amplify a hair cell's response to oscillatory mechanical stimuli. *Proc. Natl. Acad. Sci. USA.* 96:14306–14311.
68. Hudspeth, A. J., F. Jülicher, and P. Martin. 2010. A critique of the critical cochlea: Hopf—a bifurcation—is better than none. *J. Neurophysiol.* 104:1219–1229.
69. Ramamoorthy, S., D. Zha, ..., A. Fridberger. 2014. Filtering of acoustic signals within the hearing organ. *J. Neurosci.* 34:9051–9058.
70. Evans, E. F., and J. P. Wilson. 1975. Cochlear tuning properties: concurrent basilar membrane and single nerve fiber measurements. *Science.* 190:1218–1221.
71. Narayan, S. S., A. N. Temchin, ..., M. A. Ruggero. 1998. Frequency tuning of basilar membrane and auditory nerve fibers in the same cochleae. *Science.* 282:1882–1884.
72. Zwislocki, J. J. 1979. Tectorial membrane: a possible sharpening effect on the frequency analysis in the cochlea. *Acta Otolaryngol.* 87:267–269.
73. Ghaffari, R., A. J. Aranyosi, ..., D. M. Freeman. 2010. Tectorial membrane travelling waves underlie abnormal hearing in *Tectb* mutant mice. *Nat. Commun.* 1:96.
74. Bormuth, V., J. Barral, ..., P. Martin. 2014. Transduction channels' gating can control friction on vibrating hair-cell bundles in the ear. *Proc. Natl. Acad. Sci. USA.* 111:7185–7190.
75. Cheatham, M. A., and P. Dallos. 1999. Response phase: a view from the inner hair cell. *J. Acoust. Soc. Am.* 105:799–810.
76. Cheatham, M. A., and P. Dallos. 2000. The dynamic range of inner hair cell and organ of Corti responses. *J. Acoust. Soc. Am.* 107:1508–1520.
77. Cheatham, M. A., and P. Dallos. 2001. Inner hair cell response patterns: implications for low-frequency hearing. *J. Acoust. Soc. Am.* 110:2034–2044.
78. Fridberger, A., I. Tomo, ..., J. Boutet de Monvel. 2006. Imaging hair cell transduction at the speed of sound: dynamic behavior of mammalian stereocilia. *Proc. Natl. Acad. Sci. USA.* 103:1918–1923.
79. Lim, D. J. 1972. Fine morphology of the tectorial membrane. Its relationship to the organ of Corti. *Arch. Otolaryngol.* 96:199–215.
80. Ulfendahl, M., A. Flock, and E. Scarfone. 2001. Structural relationships of the unfixed tectorial membrane. *Hear. Res.* 151:41–47.
81. Cheatham, M. A., R. J. Goodyear, ..., G. P. Richardson. 2014. Loss of the tectorial membrane protein CEACAM16 enhances spontaneous, stimulus-frequency, and transiently evoked otoacoustic emissions. *J. Neurosci.* 34:10325–10338.
82. Steele, C. R., and S. Puria. 2005. Force on inner hair cell cilia. *Int. J. Solids Struct.* 42:5887–5904.
83. Steele, C. R., J. Boutet de Monvel, and S. Puria. 2009. A multiscale model of the organ of corti. *J. Mech. Mater. Struct.* 4:755–778.

## Article

# Power Dissipation in the Subtectorial Space of the Mammalian Cochlea Is Modulated by Inner Hair Cell Stereocilia

Srdjan Prodanovic,<sup>1</sup> Sheryl Gracewski,<sup>1</sup> and Jong-Hoon Nam<sup>1,2,\*</sup><sup>1</sup>Department of Mechanical Engineering and <sup>2</sup>Department of Biomedical Engineering, University of Rochester, Rochester, New York

**ABSTRACT** The stereocilia bundle is the mechano-transduction apparatus of the inner ear. In the mammalian cochlea, the stereocilia bundles are situated in the subtectorial space (STS)—a micrometer-thick space between two flat surfaces vibrating relative to each other. Because microstructures vibrating in fluid are subject to high-viscous friction, previous studies considered the STS as the primary place of energy dissipation in the cochlea. Although there have been extensive studies on how metabolic energy is used to compensate the dissipation, much less attention has been paid to the mechanism of energy dissipation. Using a computational model, we investigated the power dissipation in the STS. The model simulates fluid flow around the inner hair cell (IHC) stereocilia bundle. The power dissipation in the STS because of the presence IHC stereocilia increased as the stimulating frequency decreased. Along the axis of the stimulating frequency, there were two asymptotic values of power dissipation. At high frequencies, the power dissipation was determined by the shear friction between the two flat surfaces of the STS. At low frequencies, the power dissipation was dominated by the viscous friction around the IHC stereocilia bundle—the IHC stereocilia increased the STS power dissipation by 50- to 100-fold. There exists a characteristic frequency for STS power dissipation,  $CF_{STS}$ , defined as the frequency where power dissipation drops to one-half of the low frequency value. The IHC stereocilia stiffness and the gap size between the IHC stereocilia and the tectorial membrane determine the characteristic frequency. In addition to the generally assumed shear flow, nonshear STS flow patterns were simulated. Different flow patterns have little effect on the  $CF_{STS}$ . When the mechano-transduction of the IHC was tuned near the vibrating frequency, the active motility of the IHC stereocilia bundle reduced the power dissipation in the STS.

## INTRODUCTION

Microstructures of the cochlear sensory-epithelium vibrate in a liquid-filled cavity. To explain the high-quality factor of hearing despite the power losses because of viscous friction, Gold predicted the existence of regenerative mechanisms in the cochlea (1). After decades of research, the outer hair cells were found to provide the regenerative force for the power amplification in the cochlea (2–4). The outer hair cells should operate optimally to provide enough power to compensate for the power loss because of viscous friction (5–9). The power gain in the cochlea has been estimated/measured to explain the operating principles of the cochlear amplifier (10–12). Although power amplification and outer hair cells' power output have both been investigated in many studies, the energy dissipation in the cochlea has rarely been studied (but see 13). To understand the power balance in the cochlea, it is necessary to understand not only where and how power is generated but also where and how power is dissipated as well.

Some types of hair cells, including the IHC in the mammalian cochlea, are stimulated by viscous forces because of fluid motion. There have been theoretical studies on how the fluid flow stimulates different hair cells (14–23).

Although the mechano-transduction of certain hair cells takes advantage of the viscous flow for the stimulation, the friction of the viscous flow also dissipates energy. For example, the IHC stereocilia bundle vibrates within a few micrometer-thin fluid layer in the STS. Fluid flow on such a small scale is highly viscous; it is inevitable for the hearing organ to undergo substantial viscous friction in the STS. Although most theoretical studies do not specify where/how acoustic energy is dissipated, there were suggestions on the source of cochlear energy dissipation, especially around the tectorial membrane. The viscoelasticity of the vibrating tissues in the cochlear partition such as the tectorial membrane have been considered as one mechanism of energy dissipation (24,25). A few studies considered the viscous friction in the STS as the primary cause of energy dissipation in the mammalian cochlea (26,27). The energy dissipation in the STS was estimated from the viscous friction of a Newtonian fluid between two parallel plates representing the tectorial membrane and the reticular lamina (7,8,27). However, the STS is more complex than a fluid layer between two parallel plates in shear motion because the IHCs' stereocilia may impede or interact with the flow. Moreover, there can be modes of vibrations different from shear motion in the STS (28–30).

The objective of this work is to investigate the power dissipation in the STS through numerical simulations. The model

Submitted June 9, 2014, and accepted for publication December 15, 2014.

\*Correspondence: [jong-hoon.nam@rochester.edu](mailto:jong-hoon.nam@rochester.edu)

Editor: Jochen Guck

© 2015 by the Biophysical Society  
0006-3495/15/02/0479/10 \$2.00



incorporates STS fluid dynamics, IHC stereocilia mechanics, and mechanical feedback because of transduction channel activation/adaptations. We explain the following: 1) how mechanical and geometric properties of the stereocilia bundle affect power dissipation in the STS; 2) how power dissipation in the STS changes under different stimulation modes; and 3) how force on the fluid generated by the IHC stereocilia bundle motility affects power dissipation in the STS.

## MATERIALS AND METHODS

Similar to previous studies (15,18,23) the STS is represented by a two-dimensional rectangular fluid domain containing a hinged, rigid rod representing the IHC stereocilia bundle (Fig. 1). The rod is located in the center of the domain and the rotational spring at the rod's base represents the stereocilia bundle stiffness. Whereas the STS length is fixed at  $L = 40 \mu\text{m}$ , two different IHC stereocilia bundle heights,  $h = 2$  and  $5 \mu\text{m}$ , are considered to roughly represent the basal and the apical locations, respectively (31–33). The height of the STS,  $H$ , is  $2.1 \mu\text{m}$  (basal) and  $5.25 \mu\text{m}$  (apical) with the standard gap size.

The top and the bottom boundaries represent the tectorial membrane and the reticular lamina, respectively. The bottom boundary is fixed so the top boundary motion represents the relative motion of the tectorial membrane with respect to the reticular lamina. The right boundary represents the stereocilia bundle of the second-row outer hair cells (middle one of the three outer hair cells in Fig. 1 A). It is hinged at the top and the bottom. The left boundary represents the opening toward the inner sulcus. No-slip boundary conditions are imposed along the top, bottom, and right boundary and along the IHC stereocilia bundle. The velocity boundary condition at the left boundary (the inner sulcus) is assigned so that the net flux through the boundaries of the simulated rectangular domain becomes zero.

Although we assumed specific dimensions, geometry, and mechanical properties of the IHC stereocilia bundle, they vary across different species

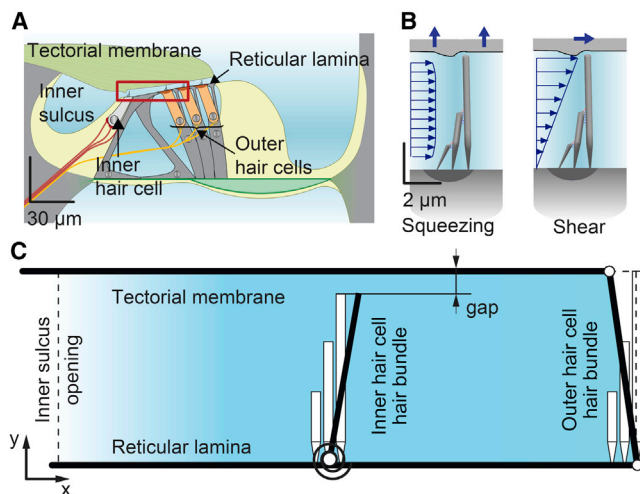


FIGURE 1 Fluid dynamics in the STS. (A) The organ of Corti. The red rectangle indicates the modeled part of STS. (B) Two different modes of STS motion resulting in squeezing and shear flow. (C) Model of the STS. The model consists of a rectangular fluid domain with boundaries representing the second-row outer hair cell stereocilia bundle, tectorial membrane, and reticular lamina, and a rigid rod hinged at the root representing the IHC stereocilia bundle. The torsional spring at the hinge represents the flexural rigidity of the IHC stereocilia. Hensen's stripe is not modeled (see Discussion). The displacements are exaggerated for illustrative purposes. To see this figure in color, go online.

and cochlear locations (32–37). The gap size between the tips of IHC stereocilia and the tectorial membrane is a key model parameter. The stiffness of the IHC stereocilia bundle was measured in several species such as Guinea pig (38), mouse (39), and rat (40). At the apical turn of the rat cochlea, the stiffness of the IHC stereocilia bundle was measured to be 2.5 to 3.5 mN/m (40). In recent studies, microprobes used to measure the bundle stiffness were found to affect hair cell mechano-transduction by unevenly deflecting the stereocilia bundle (41–44). This probe artifact should underestimate the bundle stiffness especially the IHC stereocilia bundle with a wall-like stereocilia arrangement (45). Considering the probe artifact, we used 10 mN/m for the stereocilia bundle stiffness at the apex. For the basal model, 100 mN/m was used after considering the height. Unlike the stereocilia bundle stiffness, there are no reported data about the gap size or geometry. Because these two model parameters (stiffness and gap size) were found to be important to STS fluid dynamics, we performed the parametric study for the properties that affect the STS power dissipation: IHC stereocilia stiffness and gap size between the tip of the IHC stereocilia bundle and the tectorial membrane. Finally, active mechano-transduction channels are added to the model to investigate the effect of active force feedback on the power dissipation in STS.

## Equations of fluid motion

The fluid is regarded as incompressible and the convective nonlinearities are negligible (15). The momentum and continuity equations are described in terms of fluid density ( $\rho$ ), viscosity ( $\mu$ ), pressure ( $P$ ), and velocity ( $v$ ) as in the following:

$$\rho \frac{\partial v}{\partial t} = -\nabla P + \mu \nabla^2 v, \quad (1)$$

$$\nabla \cdot v = 0. \quad (2)$$

Because the STS is subjected to cyclic stimulations, Eq. 1 and Eq. 2 can be rewritten in terms of angular frequency  $\omega$ :

$$i\omega\rho \hat{v}(x, y, \omega) = -\nabla \hat{P}(x, y, \omega) + \mu \nabla^2 \hat{v}(x, y, \omega), \quad (3)$$

$$\nabla \cdot \hat{v}(x, y, \omega) = 0, \quad (4)$$

where  $\hat{P}(x, y, \omega)$  and  $\hat{v}(x, y, \omega)$  represent complex amplitudes of the fluid pressure and velocity, respectively, and  $i$  is the imaginary unit.

## Combining active mechanics of the IHC stereocilia bundle and STS fluid dynamics

The displacement of the active IHC stereocilia bundle  $X$  is described by the following equation:

$$c_{HB} \frac{dX(t)}{dt} + k_{HB} X(t) = F(t) + F_{MT}(t), \quad (5)$$

where  $F(t)$  is the effective hydrodynamic force at the IHC stereocilia bundle tip,  $k_{HB}$  is the IHC stereocilia stiffness, and  $c_{HB}$  represents the internal viscous friction between the IHC stereocilia. The  $c_{HB}$  is expected to be small because of the minimal separating motion between stereocilia (46). The inertial force term due to stereocilia bundle mass was omitted because it is negligible compared with viscous or elastic force (see Supporting Material).  $F_{MT}$  is the active force exerted by the mechano-transduction channels (47) given as the following:

$$F_{MT}(t) = N \gamma k_G b p_O(t). \quad (6)$$

The force  $F_{MT}$  is determined by the open probability of mechano-transduction channels ( $p_o$ ), the gating spring stiffness ( $k_G$ ), the gating swing ( $b$ ), and the geometrical gain factor ( $\gamma$ ).

The active mechanism is represented by the ten-state channel kinetics model from previous work (48). The adaptation is mediated by  $\text{Ca}^{2+}$  entering through the mechano-transduction channels. The rate change of probability of the channel states ( $d\mathbf{p}/dt$ ) is described as a function of stereocilia bundle displacement,  $X$ :

$$\frac{d\mathbf{p}}{dt} = \mathbf{A}(X)\mathbf{p} + \mathbf{B}(X), \quad (7)$$

where  $\mathbf{A}$  is a  $9 \times 9$  coefficient matrix, and  $\mathbf{B}$  is a column vector. After linearization and by assuming small harmonic excitation about the resting position, Eq. 7 becomes the following:

$$\hat{\mathbf{p}}(\omega) = (i\omega \mathbf{I} - \mathbf{A}_0)^{-1}(\mathbf{A}'_0 \mathbf{p}_0 + \mathbf{B}'_0)\hat{X}(\omega), \quad (8)$$

where  $\hat{\mathbf{p}}(\omega)$  and  $\hat{X}(\omega)$  are the alternating components of  $\mathbf{p}$  and  $X$ , respectively, when stimulated at the angular frequency  $\omega$ . The variables with the subscript 0 indicate the properties evaluated at the equilibrium (resting) state.  $\mathbf{A}'_0$  and  $\mathbf{B}'_0$  are derivatives of  $\mathbf{A}$  and  $\mathbf{B}$  with respect to  $X$  at  $X_0$ , and  $\mathbf{I}$  is the identity matrix. Derivation procedures and detailed equations of the channel kinetics model are given in the [Supporting Material](#).

Considering harmonic oscillations with an angular frequency  $\omega$ , Eq. 5 becomes the following:

$$\hat{U}(\omega)(c_{HB} - i k_{HB}/\omega) = \hat{F}(\omega) + \hat{F}_{MT}(\omega), \quad (9)$$

where  $\hat{U}(\omega)$  is the alternating component of the velocity of the IHC stereocilia bundle tip. The effective hydrodynamic force  $\hat{F}(\omega)$  at the tip is obtained by dividing the total hydrodynamic torque on the IHC stereocilia bundle (integral of the pressure difference  $\Delta\hat{P}(\omega)$  across the IHC stereocilia bundle) by the bundle height  $h$ :

$$\hat{F} = \frac{1}{h} \int_0^h y \Delta\hat{P}(\omega) dy. \quad (10)$$

Hereafter, the hats will be dropped from the equations for simplicity.

## Computation

Discretization procedures and model parameters are given in the [Supporting Material](#). The overall problem size depends on the gap size between the IHC stereocilia bundle tip and the tectorial membrane because the mesh size has to be less than one-quarter of the gap size to resolve the flow pattern through the gap. The problem was solved on the BlueHive Cluster in the Center for Integrated Research Computing at the University of Rochester. It took between 0.5 to 5 h to solve for one frequency depending on the problem size.

## RESULTS

Geometric and mechanical parameters such as gap size between the IHC stereocilia bundle tip and the tectorial membrane, STS dimensions, and the IHC stereocilia stiffness determine the power dissipation in the STS. Because of the uncertainty of key model parameters such as the gap size and the IHC stereociliar stiffness, a series of parametric studies was performed. Even if we use the terms such as apical and basal model hereafter, it does not mean a specific location with well-defined characteristic frequency. They

rather refer to tall ( $5 \mu\text{m}$ ) or short ( $2 \mu\text{m}$ ) IHC stereocilia bundle (e.g., 31–33,49), respectively. Although we cannot be specific to which location/species the models correspond because of the lack of information about the STS geometry, the tall (apical) and the short (basal) model roughly represent low ( $\sim 1$  kHz) and high frequency ( $\sim 20$  kHz) locations of the mammalian cochlea, respectively. Therefore, the tall model was simulated for a frequency range between 0.1 and 10 kHz, and the short model between 1 and 100 kHz. At first, the mechano-transduction channels, the active force  $F_{MT}$  in Eq. 5, will not be included in the model. The effect of active force feedback is presented at the end of this section.

## Power dissipation in the STS

Power dissipation in the STS is evaluated as the rate of work done along the boundaries of STS. Conservation of energy for steady-state oscillation dictates that the rate of work done along the boundaries is equal to the power dissipated within the domain. The boundaries include the tectorial membrane, the outer hair cell's stereocilia bundle, and the inner sulcus. Work is not done on the reticular lamina boundary because it is stationary. The external force acting on the fluid at the boundary is equal to the internal force from the fluid acting on the boundaries. This force results from the normal and the shear stresses (50) as in the following:

$$\begin{cases} \sigma_{xx} = -P + 2\mu(\partial U/\partial x) \\ \sigma_{yy} = -P + 2\mu(\partial V/\partial y) \\ \tau_{xy} = \mu(\partial U/\partial y + \partial V/\partial x) \end{cases}, \quad (11)$$

where  $P$  is pressure, and  $U$  and  $V$  are horizontal and vertical fluid velocity components, respectively. The cycle averaged rate of work done at the outer hair cell boundary ( $P_{OHC}$ ), at the inner sulcus boundary ( $P_{IS}$ ), and at the tectorial membrane boundary ( $P_{TM}$ ) are obtained by integrating over the boundary the product of the boundary velocity and the resultant force of the stresses acting on the boundary:

$$P_{OHC} = \frac{1}{2} \text{Re} \left( - \int_0^H \sigma_{xx} U_{OHC}^* dy + \mu \int_0^H \tau_{xy} V_{OHC}^* dy \right), \quad (12)$$

$$P_{IS} = \frac{1}{2} \text{Re} \left( \int_0^H \sigma_{xx} U_{IS}^* dy - \mu \int_0^H \tau_{xy} V_{IS}^* dy \right), \quad (13)$$

$$P_{TM} = \frac{1}{2} \text{Re} \left( \mu \int_0^L \tau_{xy} U_{TM}^* dx - \int_0^L \sigma_{yy} V_{TM}^* dx \right). \quad (14)$$

The superscript asterisk indicates complex conjugate. The total power dissipated within the STS is the sum of  $P_{OHC}$ ,  $P_{TM}$  and  $P_{IS}$ , or  $P_{STS} = P_{OHC} + P_{TM} + P_{IS}$ . The result is obtained from the two-dimensional model, and it represents the power dissipation per unit depth (1  $\mu\text{m}$ ). The dissipated power is normalized by  $P_0$ , the power dissipation of the viscous shear flow between two parallel plates in terms of the plate length ( $L$ ) and the STS height ( $H$ ). See the [Supporting Material](#) for derivation.

$$P_0 = 0.5 \mu(L/H)U_0^2. \quad (15)$$

### Factors that affect power dissipation in the STS

The normalized dissipated power when the upper boundary moves with the velocity  $U = U_0 \cos(\omega t)$  is shown in [Fig. 2](#). The presence of the IHC stereocilia bundle increases the power dissipation in the STS ( $P_{STS}/P_0 > 1$ ). As the frequency  $\omega$  increases, the hydrodynamic force of the fluid dominates over elastic force of the IHC stereocilia stiffness and the normalized power dissipation asymptotically decreases to 1. As the frequency  $\omega$  decreases, the power dissipation increases to the level of dissipation that would occur if the IHC stereocilia bundle were a rigid wall. The transition between the two limiting power dissipation regimes occurs within the audible frequency range of mammals (0.1 to 100 kHz). The characteristic frequency of STS power dissipation,  $CF_{STS}$  is defined as the frequency where the power dissipation drops to one-half of the maximum value, or the phase difference between the hair bundle and the tectorial membrane becomes 45 degrees. The  $CF_{STS}$  is 0.5 and 2.8 kHz in the apical model with the gap sizes 0.5 and 1.25  $\mu\text{m}$ , respectively (indicated by solid square markers). For the basal model, the  $CF_{STS}$  is 1.5 and 28 kHz when the gap sizes are 0.1 and 0.5  $\mu\text{m}$ , respectively. When the gap size is very small (0.1 and 0.05  $\mu\text{m}$  for the apical and the basal models, respectively), the  $CF_{STS}$  is lower than the lowest simulated frequency (0.1 and 1 kHz for the apical and the basal models, respectively).

Two main parameters determining the  $CF_{STS}$  and the power dissipation are the gap size and the stiffness of the IHC stereocilia bundle. As [Fig. 2](#) shows, the gap size between the tip of the IHC stereocilia bundle and the tectorial membrane strongly affects the power dissipation. For 1 kHz stimulation to the apical model, as the gap size changes from 1.25 to 0.5 and 0.1  $\mu\text{m}$ , the normalized power dissipation changes non-monotonically from 8 to 12 and 2 ([Fig. 2 A](#)). For 20 kHz stimulation to the basal model, as the gap size decreases from 0.5 to 0.1 and 0.05  $\mu\text{m}$ , the normalized power dissipation changes monotonically from 3 to 1.5 and 1.2 ([Fig. 2 B](#)). To further investigate the relations between the power dissipation and the gap size and the IHC stereocilia stiffness, the apical model was stimulated with different stiffness and gap size values in the frequency range from 0.1 to 10 kHz

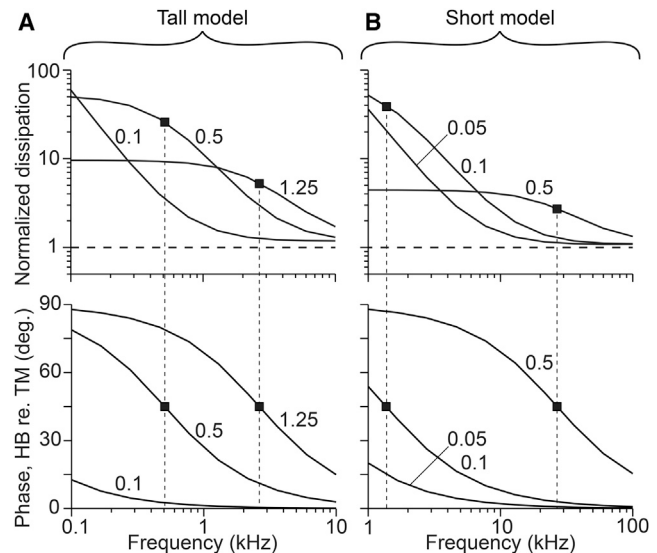


**FIGURE 2** Power dissipation in the STS and  $CF_{STS}$ . (A) Tall (apical) model. (B) Short (basal) model. Top panels: Normalized power dissipation. Bottom panels: Phase of the hair bundle with respect to the tectorial membrane. Labels on the curves indicate the size of the gap between the IHC stereocilia bundle tip and the tectorial membrane (in  $\mu\text{m}$ ). Stereocilia bundle stiffness is 10 and 100 mN/m for the tall and short models, respectively. The broken horizontal lines represent power obtained from the same model without the IHC stereocilia bundle ( $P_0$ ). The broken vertical lines indicate  $CF_{STS}$ , which correspond to half power dissipation or 45 degrees of phase difference.

([Fig. 3](#)). The normalized power dissipation increases with the stereocilia bundle stiffness, reaching the maximum value of  $\sim 200$  ([Fig. 3 A](#)). As a reference, the response that we believe reasonable (standard values: the stereocilia bundle stiffness of 10 mN/m, the best responding frequency of the location of 1 kHz, and the gap size of 0.25  $\mu\text{m}$ ) was indicated with circles in [Fig. 3, B–D](#). In the vicinity of the standard values, as the gap size increased, more power was dissipated near the assumed operating frequency (1 kHz), but at lower frequencies ( $< 1$  kHz) there exists a gap size that maximized the power dissipation ([Fig. 3 B](#)). As the stereocilia bundle stiffness increased, more power was dissipated ([Fig. 3 C](#)). Near the standard parameter values, smaller gap size and stereocilia bundle stiffness resulted in less power dissipation ([Fig. 3 D](#)). The basal model shows similar trend as the apical region (see the [Supporting Material](#)).

Since ter Kuile's kinematical analysis (51), it has been widely accepted that the IHC stereocilia bundle is stimulated by shear flow (26,37,52). However, the existence of nonshear flow in the STS has been suggested by several recent studies (28–30). We simulated nonshear stimulation modes, called squeezing modes in this work. Two simplistic squeezing modes were considered ([Fig. 4, A and B](#)). The first squeezing mode, [Fig. 4 A](#), represents the fundamental transverse vibrating mode of the tectorial membrane. The second squeezing mode, [Fig. 4 B](#), corresponds to a higher vibrating

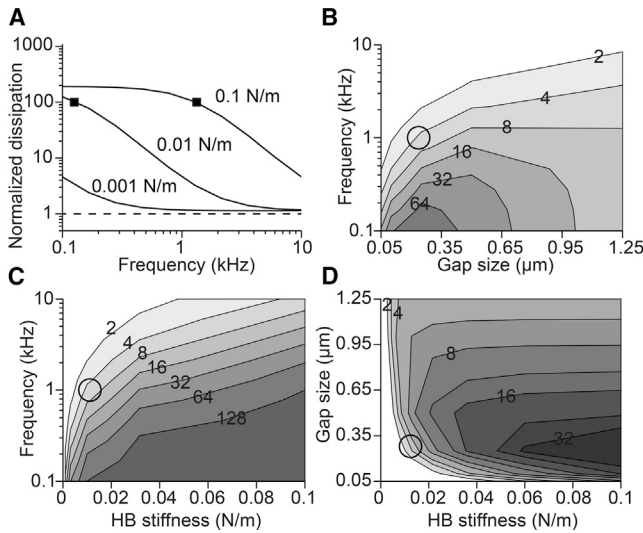


FIGURE 3 Effect of stereocilia bundle stiffness and gap size on STS power dissipation (Tall model). (A) Normalized power dissipation as function of frequency for three different values of the IHC stereocilia bundle stiffness; the gap size is  $0.25 \mu\text{m}$ . Solid square symbols indicate  $CF_{\text{STS}}$ . Contour plots of normalized power dissipation. (B) Effect of the gap size and the stimulating frequency; stiffness is  $10 \text{ mN/m}$ . (C) Effect of the stereocilia bundle stiffness and the stimulating frequency; the gap size is  $0.25 \mu\text{m}$ . (D) Effect of the stereocilia bundle stiffness and the gap size; the stimulating frequency is  $1 \text{ kHz}$ . The circles (B–D) indicate the standard parameter values of the apical model (see text). The base model result is shown in Fig. S4.

mode, and it has a zero velocity node above the IHC stereocilia bundle. Although there are reports that the outer hair cell stereocilia can elongate or shrink (53), in our study, outer hair cell stereocilia length remains unchanged.

The power dissipation of the squeezing modes is greater than that of the shear mode, although the difference is not considerable. Three modes are compared through their corresponding normalized power dissipation (Fig. 4 D). Although the motion of the tectorial membrane is distinct for each mode, the flow patterns near the IHC stereocilia are similar (Fig. 4, A–C). This similarity in flow pattern, because of the same boundary conditions at the stereocilia, may explain why the frequency-power dissipation curves are similar despite different stimulating modes (Fig. 4, D and E). Although we did not see a substantial difference in power dissipation and the  $CF_{\text{STS}}$  is nearly the same, we are hesitant to conclude that different stimulating modes have the same effect on the IHC mechano-transduction. How different modes affect the mechano-transduction may need further investigation considering the organ of Corti vibrations (8,28–30,54), but it is beyond the scope of this study.

### Can the force feedback from IHC mechano-transduction affect the STS power dissipation?

So far all the results are obtained with the stereocilia bundle without incorporating active force feedback from the me-

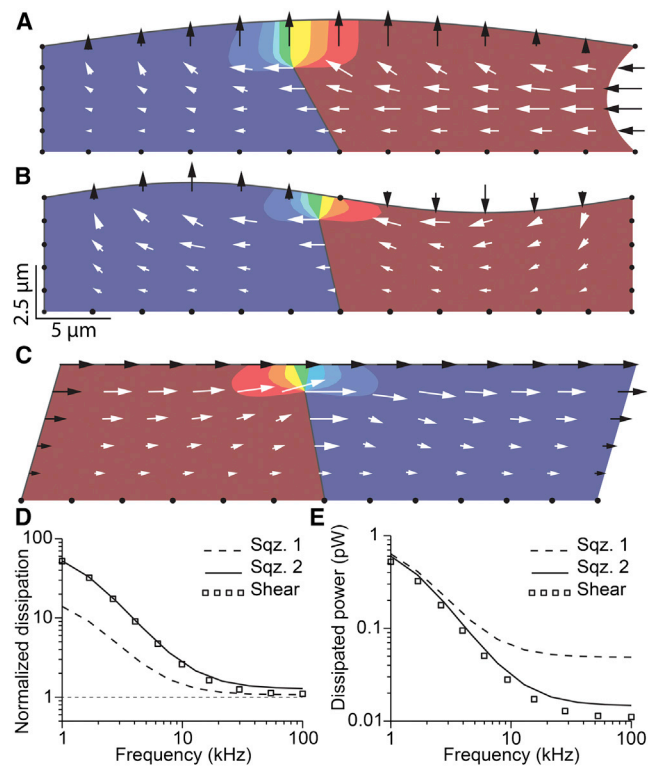


FIGURE 4 Effect of different stimulation modes (short model). Snapshots of pressure (hotter color indicates higher pressure) and velocity (arrows) fields from (A) the first squeezing mode, (B) the second squeezing mode, and (C) the shear mode. (D) Normalized power dissipation from all three modes. The squeezing modes' power dissipation is normalized by the dissipation from the same model, but without the IHC stereocilia bundle. (E) Comparison of the absolute dissipated power from the three modes. Boundary velocities were chosen so the volumetric flux through the IHC stereocilia bundle plane is constant. To see this figure in color, go online.

chano-transduction channels in the IHC stereocilia. According to measurements from nonmammalian and mammalian hair cells (e.g., 55–57), a single hair cell bundle can generate force of the order of  $100 \text{ pN}$ . Although there is no direct measurement of IHC's active force, there are measurements showing the adaptation of IHC's mechano-transduction and nonlinear mechanics (39,40,58) similar to other types of hair cells. The adaptation is considered to reflect the active mechanical feedback from the stereocilia (59,60). We investigated whether the active feedback of IHC stereocilia bundle can affect the power dissipation in the STS.

The active force of the stereocilia in our model (Eq. 6) follows conventional gating theory (47). Previous studies showed that auditory hair cells can be highly tuned at certain frequencies (48,61). Stereocilia bundle parameters were chosen within the physiologically relevant range to obtain a tuned response of the stereocilia bundle. While all other model parameters remained the same, different levels of the mechano-transduction force (different gating swings) were tested to adjust the level of tuning. First, the response

of mechano-transduction was simulated without fluid interaction; an isolated active stereocilia bundle from the tall and the short models was stimulated by a sinusoidal force (Fig. 5, A and C). As the gating swing changes from 2.9 to 2.7 and 2.0 nm, the stereocilia bundle's frequency responses change from highly-tuned to moderately-tuned and untuned.

After testing isolated bundles, the full model with fluid interaction was simulated. Active stereocilia bundle reduced the STS power dissipation, for the tall (Fig. 5 B) and the short (Fig. 5 D) models. When the stereocilia bundle is highly tuned because of active mechanical feedback from the mechano-transduction channels, the stereocilia bundle provides power to the STS rather than dissipates power: negative power dissipation around 0.55 and 3 kHz for the tall and the short models, respectively (thick solid line in Fig. 5, B and D). Moderately and poorly tuned stereocilia bundle also reduced power dissipation compared with the passive bundle.

A stereocilia bundle, tuned by active mechano-transduction channels, can provide power to the surrounding fluid. The phase relation between bundle velocity and the force the bundle exerts on the surrounding fluid explains modulation of the power dissipation in the STS by the active stereocilia bundle. The force exerted on the fluid is equal to and opposite of the force  $F$  in Eq. 5. When the STS with a highly tuned stereocilia bundle is stimulated at the tuned frequency (0.55 or 3 kHz), the force is almost in phase with the veloc-

ity and the bundle provides power per cycle to the surrounding fluid (Fig. 6 A). If the stereocilia bundle is poorly tuned, or highly tuned bundle is stimulated away from its tuned frequency (at 0.1 kHz), the force leads the velocity by a half cycle and the bundle dissipates power per cycle (Fig. 6, B–C). For the moderately tuned bundle stimulated at its tuned frequency (0.9 kHz), the force leads the velocity by a quarter cycle, and the bundle neither provides nor dissipates power (Fig. 6 D). In conclusion, properly tuned stereocilia bundle, stimulated at its tuned frequency, can greatly reduce power dissipation in the STS. A movie in the Supporting Material demonstrates the cases of Fig. 6, A and B.

## DISCUSSION

### Characteristic frequency of STS power dissipation: $CF_{STS}$

Our results show that there are two dynamic regimes of fluid-structure interaction in the STS. At high frequencies, the IHC stereocilia bundle does not impede fluid flow so that the power dissipation in the STS asymptotes to the value expected from simple viscous friction between two parallel plates. At low frequencies, the IHC stereocilia bundle is hardly deflected by the fluid flow. The stereocilia bundle behaves like a rigid wall, increasing the power dissipation by more than two orders of magnitude compared with the high-frequency case (Fig. 2, when the gap size is  $\leq 0.1 \mu\text{m}$ ). Interestingly,  $CF_{STS}$ , the frequency defining the transition point between these two regimes, is in a physiologically meaningful frequency range (between 0.1 and 100 kHz, Fig. 2) as long as the gap size is greater than 5% of the stereocilia bundle height.

The characteristic frequency of STS power dissipation,  $CF_{STS}$ , is determined by the balance between two forces—the viscous drag and the elastic restoring force of the IHC stereocilia bundle. As the bundle stiffness increases, the elastic restoring force becomes dominant so that the stereocilia bundle acts like a rigid wall impeding the fluid flow. As a result, the  $CF_{STS}$  shifts to higher value (Fig. 3 A). As the gap size decreases, the drag force experienced by the stereocilia bundle increases compared with elastic restoring force. The  $CF_{STS}$  shifts to the left along the frequency axis (Fig. 2).

### A possible role of active force from the IHC stereocilia

Our work suggests two possible ways that the mammalian hearing organ can benefit from the power dissipation because of the IHC stereocilia bundle. First, the cochlea can take advantage of a passive mechanism. Using a physiologically realistic IHC stereocilia bundle stiffness and gap size, we showed that the  $CF_{STS}$  falls within the hearing range of mammals (Fig. 2). If the  $CF_{STS}$  is near the best responding frequency of the location of the IHC, the

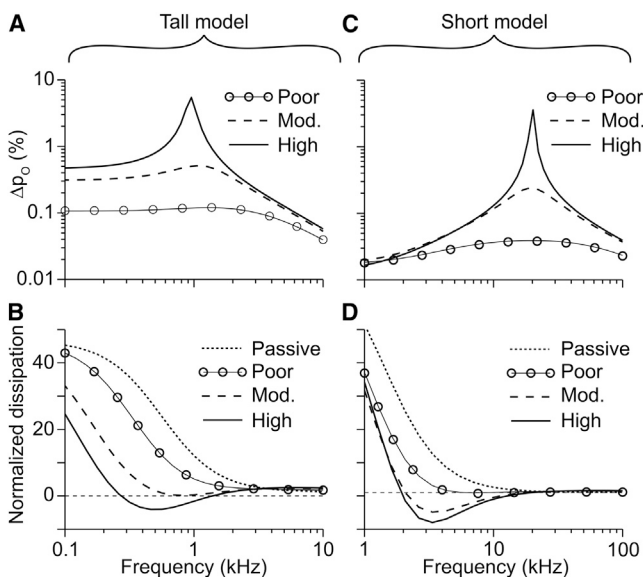


FIGURE 5 Active IHC stereocilia modulate STS power dissipation. (A) Normalized IHC transduction current ( $\Delta p_0$ ) of the tall model. (B) Normalized STS power dissipation of the tall model. (C) Normalized IHC transduction current of the short model. (D) Normalized STS power dissipation of the short model. Gap size and bundle stiffness are 0.5 and 0.1  $\mu\text{m}$  and 10 and 100 mN/m, for the tall and the short models, respectively. Results in (A) and (B) are without fluid-interaction. Four cases were simulated: three different tuning levels of the active IHC and the passive IHC.

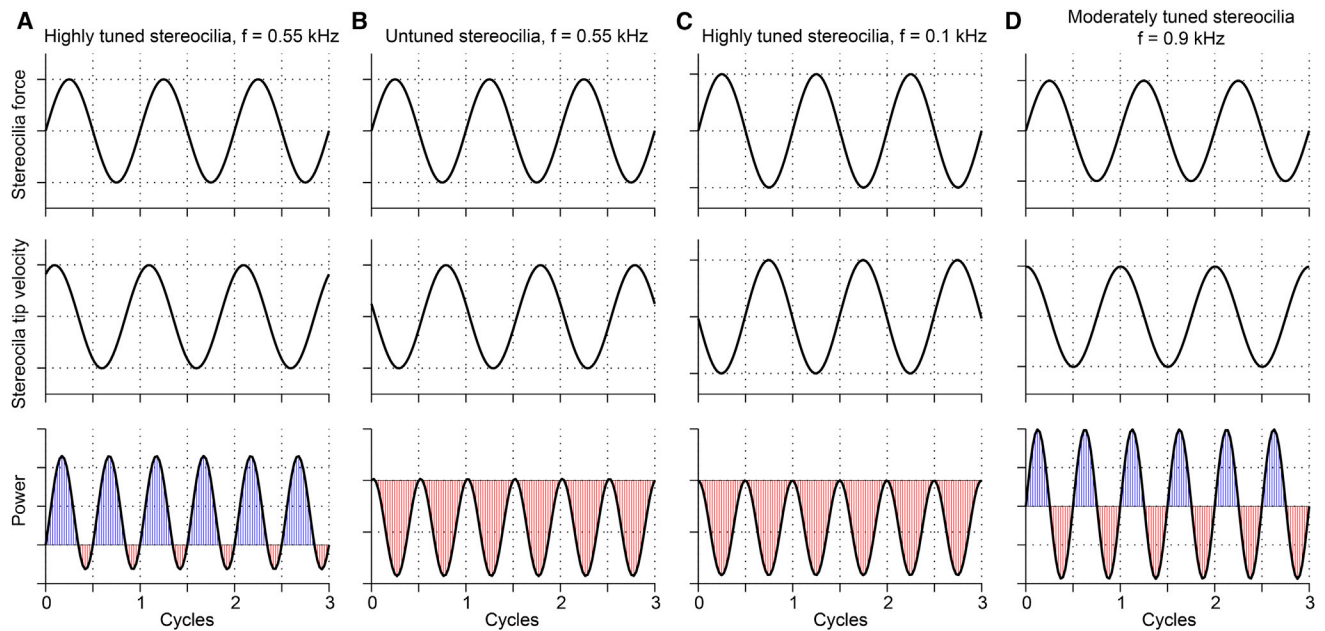


FIGURE 6 Power dissipation is determined by phase relation. (A) Highly tuned IHC stereocilia bundle ( $Q_{3dB} = 16$ ); stimulating frequency is 0.55 kHz. (B) Untuned transduction IHC stereocilia bundle; stimulating frequency is 0.55 kHz. (C) Highly tuned IHC stereocilia bundle ( $Q_{3dB} = 16$ ); stimulating frequency is 0.1 kHz. (D) Moderately tuned ( $Q_{3dB} = 1.6$ ) IHC stereocilia bundle, stimulating frequency is 0.9 kHz. Top row in all panels: force exerted by the stereocilia bundle on the surrounding fluid. Middle row in all panels: velocity of the stereocilia tip. Blue color indicates power transmitted to the fluid from the stereocilia bundle; red color indicates dissipated power (shaded area above and below the horizontal line, respectively). To see this figure in color, go online.

additional power dissipation because of the IHC stereocilia can sharpen the frequency tuning by acting as a high-pass filter. This idea of the IHC stereocilia bundle as a high-pass filter is in agreement with previous studies (14,17,19). Secondly, the mammalian cochlea can use the active mechanism of the IHC stereocilia bundle to modulate power dissipation. It is known that the bundle has at least two active adaptation mechanisms distinguished by their operating speeds (41,62,63). It has been measured/estimated that a single stereocilia bundle can generate at least tens of pN of force (40,47,55,64). Although the active stereocilia bundle mechanics of IHC is less investigated compared with nonhearing hair cells or outer hair cells, the adaptation of mechano-transduction current (e.g., 65) and the dependence of stereocilia bundle mechanics on mechano-transduction (39,40) indicate that the IHC stereocilia can also generate forces similar to other types of hair cells. In this study, the single-channel gating force (the product of the gating swing and gating spring stiffness), the force generated by a single channel because of its configuration change (47), ranges between 7 and 12 pN, which is comparable with the values in other studies with mammalian cochlear hair cell (48,66). After considering the number of channels and the geometrical gain, this single-channel gating force corresponds to  $\sim 100$  and 250 pN per stereocilia bundle of the tall and the short models, respectively.

When the active force is applied with proper timing (phase) with respect to the external stimulation, our results (Figs. 5 and 6) show that the IHC stereocilia bundle provides

energy instead of dissipating it. This seems surprising in that a stereocilia bundle can overcome arguably primary energy dissipation (26,27) in the cochlea. But, it is reasonable considering that the STS viscous friction is comparable with the viscous friction that a stereocilia bundle is subjected to in a hemi-infinite fluid space (48). For example, the friction coefficient of the STS (without the IHC stereocilia bundle) is  $\sim 50$  nNs/m ( $\mu Lb/H$ , where  $b$  is the width of a hair cell). This is comparable with the viscous friction experienced by a sphere with  $d = 8 \mu\text{m}$  ( $3\pi\mu d$ ). It was shown that the bullfrog sacculus stereocilia bundle overcomes the viscous drag over 100 nNs/m to oscillate spontaneously, and the actuator is considered the mechano-transduction channels in the stereocilia bundle (67).

Despite our simulated result of negative damping in the STS because of stereocilia bundle's feedback force, we do not argue that this instability exists in the cochlea. Our purpose was to explore physiologically possible range of stereocilia bundle's mechanical feedback. A conservative conclusion of our result is that the IHC stereocilia bundle (despite its tuning) can actively modulate the power dissipation in the STS through its mechanical feedback originating from its mechano-transduction channels. The modulation is more effective when the bundle operates near its unstable state (68).

### Inner hair cell tuning

The tuned IHC mechano-transduction in Fig. 5 is reminiscent of the nearly obsolete concept of a second filter (but,

see 69). A second filter in the cochlea implies any mechanism that is responsible for the difference between the mechanical tuning measured at the basilar membrane and the neural tuning of auditory nerve fibers (70). This concept has lost favor as the sharpness of the neural tuning and the mechanical tuning were found to be comparable (71). Our work was not intended to revisit the idea of a second filter because our analyses were limited to a subdomain of the entire cochlear mechanics. That said, it was shown that a small change in the channel kinetics can change the power dissipation in the STS dramatically (Fig. 5) by adjusting the phase of the active force from the stereocilia bundle with respect to the fluid flow (Fig. 6). In other words, the IHC stereocilia bundle acting as an active damper has a potential to affect overall cochlear mechanics.

There are two conditions under which the IHC can contribute to cochlear tuning through its modulation of power dissipation. First, the IHC can contribute to the mechanical tuning of the cochlear partition (the first filter) provided that this STS power dissipation dominates the overall power dissipation in the cochlear partition. Second, if the tectorial membrane vibrates independent of the basilar membrane (72,73), the IHC's modulation of STS power dissipation may contribute to a second filter through the mechanism suggested by Zwislocki (72).

The extent and magnitude of the power modulation by the IHC stereocilia bundle are determined by two factors—the force and the timing. In our work, the single-channel gating force determined the magnitude of the active force generated in the IHC stereocilia. The single-channel gating force is linearly proportional to the gating swing (47). By simulating different gating swing values, we showed the effect of the stereocilia bundle motility (Fig. 5). The timing (phase) of the active force application with respect to the fluid flow is determined by the characteristic frequency of stereocilia bundle. Fig. 6 demonstrates the effect of this timing. There are different theories on how the characteristic frequency of the hair cell mechano-transduction is determined (e.g., 48,66,74). The characteristic frequency in our model is determined by the adaptation speed, the activation speed of the mechano-transduction channel and the stereocilia bundle stiffness. Although a specific mechano-transduction model was used, our finding holds despite different mechano-transduction theories provided that an appropriate stereocilia bundle force (Fig. 5) is applied with the right timing (Fig. 6).

It is unclear whether the IHC's mechano-transduction is in phase with the basilar membrane displacement or velocity. Available data indicate that the phase relationship depends on the stimulation level and the stimulation frequency (75–78). Our results show that the IHC stereocilia bundle displacement is in phase with the STS shear displacement at high frequencies, but with STS shear velocity at low frequencies (Fig. 2). The frequency-dependence varies according to the bundle's mechanical feedback

(Figs. 5 and 6). For a better comparison with experimental results, however, the STS fluid dynamics should be solved in the context of whole organ of Corti mechanics.

### Limitations of this study—the importance of STS anatomy

Although there are available data regarding the IHC stereocilia bundle stiffness (39,58), there is very limited information about how the gap between the tips of the IHC stereocilia and the tectorial membrane is shaped. In particular, there is a characteristic ridge on the undersurface of the tectorial membrane, in the vicinity of the IHC stereocilia tips, known as the Hensen's stripe (79). The size, position, and connectivity to the IHC stereocilia bundle and reticular lamina are not well characterized. For example, whether Hensen's stripe is connected to the IHC stereocilia is unclear (35,80). In mice, the Hensen's stripe was not observed in apical (low frequency) locations of the cochlea as it was in basal locations (81).

Steele and his colleagues considered that the mechanical role of the Hensen's stripe is to provide a strong viscous coupling between the tectorial membrane and the IHC stereocilia (82,83). In their work, the computational cost of fluid dynamical analysis in the STS was reduced by deriving the viscous coupling term assuming Poiseuille flow between a plate (Hensen's stripe) and a cylinder (stereocilia tips). Although we did not include the Hensen's stripe because of anatomical uncertainty and computational complexity, based on Steele et al.'s work, we can presume its effect. If the Hensen's stripe has a significant depth and is close enough to the IHC stereocilia (comparable with the gap size), it will increase the viscous coupling between the tectorial membrane and the IHC stereocilia similar to the decrease in the gap size in our work.

### SUPPORTING MATERIAL

Supporting Material, four figures, one table, and two movies are available at [http://www.biophysj.org/biophysj/supplemental/S0006-3495\(14\)04774-2](http://www.biophysj.org/biophysj/supplemental/S0006-3495(14)04774-2).

### ACKNOWLEDGMENTS

This work was supported by NSF CMMI-1233595 and the University of Rochester via an HSCCI award.

### REFERENCES

1. Gold, T. 1948. Hearing. 2. The physical basis of the action of the cochlea. *Proc. R. Soc. Ser. B-Bio. Sci.* 135:492–498.
2. Brownell, W. E., C. R. Bader, ..., Y. de Ribaupierre. 1985. Evoked mechanical responses of isolated cochlear outer hair cells. *Science*. 227:194–196.
3. Ashmore, J. 2008. Cochlear outer hair cell motility. *Physiol. Rev.* 88:173–210.
4. Dallos, P. 2008. Cochlear amplification, outer hair cells and prestin. *Curr. Opin. Neurobiol.* 18:370–376.

5. Ospeck, M., X. X. Dong, and K. H. Iwasa. 2003. Limiting frequency of the cochlear amplifier based on electromotility of outer hair cells. *Biophys. J.* 84:739–749.
6. Rabbitt, R. D., S. Clifford, ..., W. E. Brownell. 2009. Power efficiency of outer hair cell somatic electromotility. *PLoS Comput. Biol.* 5:e1000444.
7. Sul, B., and K. H. Iwasa. 2009. Amplifying effect of a release mechanism for fast adaptation in the hair bundle. *J. Acoust. Soc. Am.* 126:4–6.
8. Nam, J. H., and R. Fettiplace. 2012. Optimal electrical properties of outer hair cells ensure cochlear amplification. *PLoS ONE.* 7:e50572.
9. Ramamoorthy, S., and A. L. Nuttall. 2012. Outer hair cell somatic electromotility in vivo and power transfer to the organ of Corti. *Biophys. J.* 102:388–398.
10. Shera, C. A. 2007. Laser amplification with a twist: traveling-wave propagation and gain functions from throughout the cochlea. *J. Acoust. Soc. Am.* 122:2738–2758.
11. Fisher, J. A. N., F. Nin, ..., A. J. Hudspeth. 2012. The spatial pattern of cochlear amplification. *Neuron.* 76:989–997.
12. Dong, W., and E. S. Olson. 2013. Detection of cochlear amplification and its activation. *Biophys. J.* 105:1067–1078.
13. Dong, W., and E. S. Olson. 2009. In vivo impedance of the gerbil cochlear partition at auditory frequencies. *Biophys. J.* 97:1233–1243.
14. Weiss, T. F., and R. Leong. 1985. A model for signal transmission in an ear having hair cells with free-standing stereocilia. III. Micromechanical stage. *Hear. Res.* 20:157–174.
15. Freeman, D. M., and T. F. Weiss. 1990. Superposition of hydrodynamic forces on a hair bundle. *Hear. Res.* 48:1–15.
16. Freeman, D. M., and T. F. Weiss. 1990. Hydrodynamic forces on hair bundles at low frequencies. *Hear. Res.* 48:17–30.
17. Freeman, D. M., and T. F. Weiss. 1990. Hydrodynamic forces on hair bundles at high frequencies. *Hear. Res.* 48:31–36.
18. Freeman, D. M., and T. F. Weiss. 1988. The role of fluid inertia in mechanical stimulation of hair cells. *Hear. Res.* 35:201–207.
19. Zetes, D. E., and C. R. Steele. 1997. Fluid-structure interaction of the stereocilia bundle in relation to mechanotransduction. *J. Acoust. Soc. Am.* 101:3593–3601.
20. Nam, J. H., J. R. Cotton, and J. W. Grant. 2005. Effect of fluid forcing on vestibular hair bundles. *J. Vestib. Res.* 15:263–278.
21. Shatz, L. F. 2004. The effect of hair bundle shape on hair bundle hydrodynamics of non-mammalian inner ear hair cells for the full frequency range. *Hear. Res.* 195:41–53.
22. Shatz, L. F. 2000. The effect of hair bundle shape on hair bundle hydrodynamics of inner ear hair cells at low and high frequencies. *Hear. Res.* 141:39–50.
23. Billone, M., and S. Raynor. 1973. Transmission of radial shear forces to cochlear hair cells. *J. Acoust. Soc. Am.* 54:1143–1156.
24. Sellon, J. B., R. Ghaffari, ..., D. M. Freeman. 2014. Porosity controls spread of excitation in tectorial membrane traveling waves. *Biophys. J.* 106:1406–1413.
25. Jones, G. P., V. A. Lukashkina, ..., A. N. Lukashkin. 2013. Frequency-dependent properties of the tectorial membrane facilitate energy transmission and amplification in the cochlea. *Biophys. J.* 104:1357–1366.
26. Allen, J. B. 1980. Cochlear micromechanics—a physical model of transduction. *J. Acoust. Soc. Am.* 68:1660–1670.
27. Mammano, F., and R. Nobili. 1993. Biophysics of the cochlea: linear approximation. *J. Acoust. Soc. Am.* 93:3320–3332.
28. Guinan, Jr., J. J. 2012. How are inner hair cells stimulated? Evidence for multiple mechanical drives. *Hear. Res.* 292:35–50.
29. Nowotny, M., and A. W. Gummer. 2006. Nanomechanics of the subtectorial space caused by electromechanics of cochlear outer hair cells. *Proc. Natl. Acad. Sci. USA.* 103:2120–2125.
30. Nowotny, M., and A. W. Gummer. 2011. Vibration responses of the organ of Corti and the tectorial membrane to electrical stimulation. *J. Acoust. Soc. Am.* 130:3852–3872.
31. Furness, D. N., S. Mahendrasingam, ..., C. M. Hackney. 2008. The dimensions and composition of stereociliary rootlets in mammalian cochlear hair cells: comparison between high- and low-frequency cells and evidence for a connection to the lateral membrane. *J. Neurosci.* 28:6342–6353.
32. Lim, D. J. 1980. Cochlear anatomy related to cochlear micromechanics. A review. *J. Acoust. Soc. Am.* 67:1686–1695.
33. Yarin, Y. M., A. N. Lukashkin, ..., T. Zahnert. 2014. Tonotopic morphometry of the lamina reticularis of the guinea pig cochlea with associated microstructures and related mechanical implications. *J. Assoc. Res. Otolaryngol.* 15:1–11.
34. Lim, D. J. 1986. Functional structure of the organ of Corti: a review. *Hear. Res.* 22:117–146.
35. Rueda, J., R. Cantos, and D. J. Lim. 1996. Tectorial membrane-organ of Corti relationship during cochlear development. *Anat. Embryol. (Berl.)*. 194:501–514.
36. Edge, R. M., B. N. Evans, ..., P. Dallos. 1998. Morphology of the un-fixed cochlea. *Hear. Res.* 124:1–16.
37. Dallos, P. 2003. Organ of Corti kinematics. *J. Assoc. Res. Otolaryngol.* 4:416–421.
38. Strelieff, D., and A. Flock. 1984. Stiffness of sensory-cell hair bundles in the isolated guinea pig cochlea. *Hear. Res.* 15:19–28.
39. Russell, I. J., M. Kössl, and G. P. Richardson. 1992. Nonlinear mechanical responses of mouse cochlear hair bundles. *Proc. Biol. Sci.* 250:217–227.
40. Beurg, M., J. H. Nam, ..., R. Fettiplace. 2008. The actions of calcium on hair bundle mechanics in mammalian cochlear hair cells. *Biophys. J.* 94:2639–2653.
41. Peng, A. W., T. Effertz, and A. J. Ricci. 2013. Adaptation of mammalian auditory hair cell mechanotransduction is independent of calcium entry. *Neuron.* 80:960–972.
42. Karavitaki, K. D., and D. Corey. 2014. A new probe for cochlear hair bundle stimulation. In Association for Research in Otolaryngology Midwinter Meeting, San Diego, CA.
43. Indzhukulian, A. A., R. Stepanyan, ..., G. I. Frolenkov. 2013. Molecular remodeling of tip links underlies mechanosensory regeneration in auditory hair cells. *PLoS Biol.* 11:e1001583.
44. Corns, L. F., S. L. Johnson, ..., W. Marcotti. 2014. Calcium entry into stereocilia drives adaptation of the mechano-electrical transducer current of mammalian cochlear hair cells. *Proc. Natl. Acad. Sci. USA.* 111:14918–14923.
45. Langer, M. G., S. Fink, ..., J. P. Ruppertsberg. 2001. Lateral mechanical coupling of stereocilia in cochlear hair bundles. *Biophys. J.* 80:2608–2621.
46. Kozlov, A. S., J. Baumgart, ..., A. J. Hudspeth. 2011. Forces between clustered stereocilia minimize friction in the ear on a subnanometre scale. *Nature.* 474:376–379.
47. Howard, J., and A. J. Hudspeth. 1988. Compliance of the hair bundle associated with gating of mechano-electrical transduction channels in the bullfrog's saccular hair cell. *Neuron.* 1:189–199.
48. Nam, J. H., and R. Fettiplace. 2008. Theoretical conditions for high-frequency hair bundle oscillations in auditory hair cells. *Biophys. J.* 95:4948–4962.
49. Nadol, Jr., J. B. 1988. Comparative anatomy of the cochlea and auditory nerve in mammals. *Hear. Res.* 34:253–266.
50. Batchelor, G. K. 1967. An Introduction to Fluid Dynamics. Cambridge University Press, Cambridge, UK.
51. ter Kuile, E. 1900. Die übertragung der energie von der grundmembran auf die haarzellen. *Pflügers Archiv. European J. Physiol.* 79:146–157.
52. Rhode, W. S., and C. D. Geisler. 1967. Model of the displacement between opposing points on the tectorial membrane and reticular lamina. *J. Acoust. Soc. Am.* 42:185–190.
53. Hakizimana, P., W. E. Brownell, ..., A. Fridberger. 2012. Sound-induced length changes in outer hair cell stereocilia. *Nat. Commun.* 3:1094.

54. Nam, J. H. 2014. Microstructures in the organ of Corti help outer hair cells form traveling waves along the cochlear coil. *Biophys. J.* 106:2426–2433.
55. Kennedy, H. J., A. C. Crawford, and R. Fettiplace. 2005. Force generation by mammalian hair bundles supports a role in cochlear amplification. *Nature.* 433:880–883.
56. Ricci, A. J., A. C. Crawford, and R. Fettiplace. 2002. Mechanisms of active hair bundle motion in auditory hair cells. *J. Neurosci.* 22:44–52.
57. Bozovic, D., and A. J. Hudspeth. 2003. Hair-bundle movements elicited by transepithelial electrical stimulation of hair cells in the sacculus of the bullfrog. *Proc. Natl. Acad. Sci. USA.* 100:958–963.
58. Beurg, M., M. G. Evans, ..., R. Fettiplace. 2006. A large-conductance calcium-selective mechanotransducer channel in mammalian cochlear hair cells. *J. Neurosci.* 26:10992–11000.
59. Assad, J. A., and D. P. Corey. 1992. An active motor model for adaptation by vertebrate hair cells. *J. Neurosci.* 12:3291–3309.
60. Ricci, A. J., A. C. Crawford, and R. Fettiplace. 2000. Active hair bundle motion linked to fast transducer adaptation in auditory hair cells. *J. Neurosci.* 20:7131–7142.
61. Choe, Y., M. O. Magnasco, and A. J. Hudspeth. 1998. A model for amplification of hair-bundle motion by cyclical binding of Ca<sup>2+</sup> to mechano-electrical-transduction channels. *Proc. Natl. Acad. Sci. USA.* 95:15321–15326.
62. Eatock, R. A. 2000. Adaptation in hair cells. *Annu. Rev. Neurosci.* 23:285–314.
63. Fettiplace, R., and A. J. Ricci. 2003. Adaptation in auditory hair cells. *Curr. Opin. Neurobiol.* 13:446–451.
64. Jaramillo, F., and A. J. Hudspeth. 1993. Displacement-clamp measurement of the forces exerted by gating springs in the hair bundle. *Proc. Natl. Acad. Sci. USA.* 90:1330–1334.
65. Kros, C. J., A. Rüscher, and G. P. Richardson. 1992. Mechano-electrical transducer currents in hair cells of the cultured neonatal mouse cochlea. *Proc. Biol. Sci.* 249:185–193.
66. Tinevez, J. Y., F. Jülicher, and P. Martin. 2007. Unifying the various incarnations of active hair-bundle motility by the vertebrate hair cell. *Biophys. J.* 93:4053–4067.
67. Martin, P., and A. J. Hudspeth. 1999. Active hair-bundle movements can amplify a hair cell's response to oscillatory mechanical stimuli. *Proc. Natl. Acad. Sci. USA.* 96:14306–14311.
68. Hudspeth, A. J., F. Jülicher, and P. Martin. 2010. A critique of the critical cochlea: Hopf—a bifurcation—is better than none. *J. Neurophysiol.* 104:1219–1229.
69. Ramamoorthy, S., D. Zha, ..., A. Fridberger. 2014. Filtering of acoustic signals within the hearing organ. *J. Neurosci.* 34:9051–9058.
70. Evans, E. F., and J. P. Wilson. 1975. Cochlear tuning properties: concurrent basilar membrane and single nerve fiber measurements. *Science.* 190:1218–1221.
71. Narayan, S. S., A. N. Temchin, ..., M. A. Ruggero. 1998. Frequency tuning of basilar membrane and auditory nerve fibers in the same cochleae. *Science.* 282:1882–1884.
72. Zwislocki, J. J. 1979. Tectorial membrane: a possible sharpening effect on the frequency analysis in the cochlea. *Acta Otolaryngol.* 87:267–269.
73. Ghaffari, R., A. J. Aranyosi, ..., D. M. Freeman. 2010. Tectorial membrane travelling waves underlie abnormal hearing in *Tectb* mutant mice. *Nat. Commun.* 1:96.
74. Bormuth, V., J. Barral, ..., P. Martin. 2014. Transduction channels' gating can control friction on vibrating hair-cell bundles in the ear. *Proc. Natl. Acad. Sci. USA.* 111:7185–7190.
75. Cheatham, M. A., and P. Dallos. 1999. Response phase: a view from the inner hair cell. *J. Acoust. Soc. Am.* 105:799–810.
76. Cheatham, M. A., and P. Dallos. 2000. The dynamic range of inner hair cell and organ of Corti responses. *J. Acoust. Soc. Am.* 107:1508–1520.
77. Cheatham, M. A., and P. Dallos. 2001. Inner hair cell response patterns: implications for low-frequency hearing. *J. Acoust. Soc. Am.* 110:2034–2044.
78. Fridberger, A., I. Tomo, ..., J. Boutet de Monvel. 2006. Imaging hair cell transduction at the speed of sound: dynamic behavior of mammalian stereocilia. *Proc. Natl. Acad. Sci. USA.* 103:1918–1923.
79. Lim, D. J. 1972. Fine morphology of the tectorial membrane. Its relationship to the organ of Corti. *Arch. Otolaryngol.* 96:199–215.
80. Ulfendahl, M., A. Flock, and E. Scarfone. 2001. Structural relationships of the unfixed tectorial membrane. *Hear. Res.* 151:41–47.
81. Cheatham, M. A., R. J. Goodyear, ..., G. P. Richardson. 2014. Loss of the tectorial membrane protein CEACAM16 enhances spontaneous, stimulus-frequency, and transiently evoked otoacoustic emissions. *J. Neurosci.* 34:10325–10338.
82. Steele, C. R., and S. Puria. 2005. Force on inner hair cell cilia. *Int. J. Solids Struct.* 42:5887–5904.
83. Steele, C. R., J. Boutet de Monvel, and S. Puria. 2009. A multiscale model of the organ of corti. *J. Mech. Mater. Struct.* 4:755–778.

## Supporting Material

### Power dissipation in the sub-tectorial space of the mammalian cochlea modulated by inner hair cell stereocilia

Srdjan Prodanovic<sup>1</sup>, Sheryl Gracewski<sup>1</sup>, and Jong-Hoon Nam<sup>1,2</sup>

<sup>1</sup>Department of Mechanical Engineering, <sup>2</sup>Department of Biomedical Engineering

University of Rochester, Rochester, NY 14627, USA

#### Discretization of governing equations

Equations 1, 2 and 7 subject to the no-slip boundary conditions are solved numerically on a staggered grid (1) shown in Fig. S1. Pressure is defined in the cell midpoints, denoted by (a, b) coordinate pair. The horizontal velocity component ( $U$ ) is placed on the vertical cell interfaces (a', b), and the vertical velocity component ( $V$ ) is placed on the horizontal cell interfaces (a, b'). Pressure and the two velocity components are defined on three different grids. The computational domain is divided into  $N_x$  by  $N_y$  cells. The IHC stereocilia bundle is represented as the vertical cell interface, impermeable for the fluid, located  $N_{0.5x} = 0.5 \times N_x$  cells away from the right boundary. There are  $N_{HB}$  cells along the IHC stereocilia height. The grid is uniform in both  $x$  and  $y$  direction with a horizontal grid spacing of  $\Delta x$  and vertical spacing of  $\Delta y$ .

The pressure gradient will be discretized by the first order scheme and the Laplacian with the second order central difference scheme. Applying the  $x$  component of Eq. 1 at the  $(n, m)$   $U$  velocity nodes and introducing difference approximations for  $n = 1, 2 \dots N_x - 1$  and for  $m = 1, 2 \dots N_y$ , we obtain the following finite difference equation

$$\mu \left( \frac{U_{n-1,m} - 2U_{n,m} + U_{n+1,m}}{\Delta x^2} + \frac{U_{n,m-1} - 2U_{n,m} + U_{n,m+1}}{\Delta y^2} \right) - i\omega\rho U_{n,m} - \frac{P_{n+1,m} - P_{n,m}}{\Delta x} = 0. \quad (\text{A1})$$

Applying the  $y$  component of Eq. 1 at the  $(n, m)$   $V$  velocity nodes, for  $n = 1, 2 \dots N_x$  and  $m = 1, 2 \dots N_y - 1$  we obtain

$$\mu \left( \frac{V_{n-1,m} - 2V_{n,m} + V_{n+1,m}}{\Delta x^2} + \frac{V_{n,m-1} - 2V_{n,m} + V_{n,m+1}}{\Delta y^2} \right) - i\omega\rho U_{n,m} - \frac{P_{n,m+1} - P_{n,m}}{\Delta x} = 0. \quad (\text{A2})$$

The continuity equation, Eq. 2, at the  $(n, m)$  pressure nodes, for  $n = 1, 2 \dots N_x$  and  $m = 1, 2 \dots N_y$  is



**Power dissipation of the flow between two parallel plates**

A viscous fluid of dynamic viscosity  $\mu$  is placed between two parallel plates at distance  $H$  from each other, Fig. S2A. The bottom plate is fixed, and the upper plate is moving with velocity  $U = U_0 \cos(\omega t)$ . Third dimension,  $t$  is given 1.

Energy loss in this system occurs only under top plate due to viscous friction. If the fluid is Newtonian than shear stress is given as

$$\tau = \mu \frac{\partial U}{\partial y} \Big|_{y=H} = \mu \frac{U_0 \cos(\omega t)}{H} \tag{A10}$$

The shear force acting on the top plate is

$$F = \tau L t = \mu \frac{L}{H} U_0 \cos(\omega t) \tag{A11}$$

The work done by this force over a single cycle is

$$W = \int_0^T F U dt = \mu \frac{L}{H} U_0 \int_0^{\frac{2\pi}{\omega}} \cos^2(\omega t) dt = \mu \frac{L}{H} U_0 \frac{\pi}{\omega} \tag{A12}$$

The dissipated power per cycle is then

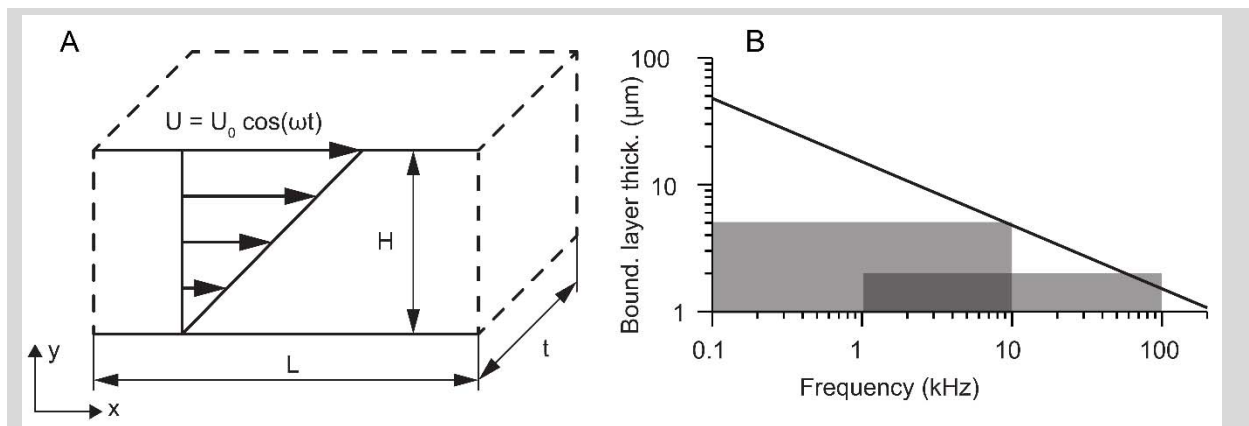


**Figure S2.** (A) Viscous Newtonian fluid between two parallel plates. The bottom plate is stationary while the top plate oscillates. (B) The line represents the boundary layer thickness in water, according to Eq. A14. Two shaded areas indicate the simulated span of the tall (5  $\mu\text{m}$ ) and the short (2  $\mu\text{m}$ ) model, respectively. The tall model stays under the boundary layer within the simulated range (0.1-10 kHz). The short model's boundary layer thickness falls below the STS height above 60 kHz.

$$P_0 = \frac{W}{T} = \frac{\mu U_0 \pi}{H \omega} \frac{\omega}{2\pi} = 0.5 \mu (L/H) U_0^2 \quad (\text{A13})$$

For low Reynolds number, the oscillatory boundary layer thickness  $\delta$  is approximated as in (2)

$$\delta = \sqrt{\mu / (\pi \rho f)} \quad (\text{A14})$$

where,  $f$  is the frequency in Hz.

Fig S2B shows that the oscillatory boundary layer thickness is larger than the STS height for most of the simulated frequencies; it reaches 2  $\mu\text{m}$  for  $\sim 60$  kHz stimulation. Even when the boundary layer thickness drops below the STS height at the highest simulated frequency (100 kHz), the difference in the power dissipation between nonlinear and linear shear flow does not exceed 20%.

#### **Inertial term in the equation of motion of the stereocilia bundle is negligible**

The inertia of the stereocilia bundle was ignored because it is negligible compared to the viscous and the elastic force. Because the inertial effect is greatest at the highest frequency, conservatively, we consider a case of 100 kHz stimulation to the hair bundle properties at 20 kHz location. The stiffness of the hair bundle,  $k$ , is 100 mN/m, and the damping coefficient of the hair bundle,  $c$ , is 10 nN s/m (comparable to 4  $\mu\text{m}$  sphere). The mass density of the hair bundle will be assumed to be equal to water density and the volume will be calculated by assuming a box shape,  $2 \times 1.5 \times 8 \mu\text{m}$ . This results in the mass of 24 pg ( $24 \times 10^{-15}$  kg).

With these physiologically reasonable values, when a hair bundle vibrates with the amplitude of 1 nm at 100 kHz, the inertial force is  $9.5 \times 10^{-18}$  N, the viscous force is  $1.3 \times 10^{-14}$  N and the elastic force is  $1 \times 10^{-7}$  N. The inertial term is at least 3 orders of magnitude smaller than the other two force terms. At the low frequency location, the inertial term is even more negligible while the viscous and the elastic terms become comparable.

### Mechano-transduction channel kinetics

Our model assumes a mechano-transduction channel to have four  $\text{Ca}^{2+}$ -binding sites and two configurations (open or closed, Fig S3). Using the constraint  $\sum_{i=0}^9 p_i = 1$  to express one state probability as a function of others as  $p_1 = 1 - \sum_{i=2}^9 p_i$ , the equations of the kinetic scheme of the 10-state channel can be reduced to the nonsingular form

$$\frac{d\mathbf{p}}{dt} = \mathbf{A}(X)\mathbf{p} + \mathbf{B}(X). \quad (\text{A15})$$

where  $\mathbf{p}$  is the vector column of state probabilities,  $\mathbf{A}$  is  $9 \times 9$  coefficient matrix that is a function of stereocilia bundle displacement  $X$ , and  $\mathbf{B}$  is a column vector. Matrices  $\mathbf{A}$  and  $\mathbf{B}$  are

$$\mathbf{A} = - \begin{bmatrix} k_{21} + k_{23} + k_{29} - k_{12} & k_{12} - k_{32} & k_{12} & k_{12} & k_{12} & k_{12} & k_{12} & k_{12} - k_{92} & k_{12} \\ -k_{23} & k_{32} + k_{34} + k_{38} & -k_{34} & 0 & 0 & 0 & -k_{83} & 0 & 0 \\ 0 & -k_{34} & k_{43} + k_{45} + k_{47} & -k_{54} & 0 & -k_{74} & 0 & 0 & 0 \\ 0 & 0 & -k_{45} & k_{54} + k_{56} & -k_{65} & 0 & 0 & 0 & 0 \\ 0 & 0 & 0 & -k_{56} & k_{56} + k_{67} & -k_{76} & 0 & 0 & 0 \\ 0 & 0 & -k_{47} & 0 & -k_{67} & k_{74} + k_{76} + k_{78} & -k_{87} & 0 & 0 \\ 0 & -k_{38} & 0 & 0 & 0 & -k_{78} & k_{83} + k_{87} + k_{89} & -k_{98} & 0 \\ -k_{29} & 0 & 0 & 0 & 0 & 0 & -k_{89} & k_{92} + k_{98} + k_{910} & -k_{09} \\ k_{10} & k_{10} - k_{90} & k_{01} + k_{09} + k_{10} \end{bmatrix} \quad (\text{A16})$$

$$\mathbf{B} = [-k_{12} \quad 0 \quad -k_{10}]^T, \quad (\text{A17})$$

and column vector  $\mathbf{p}$  is

$$\mathbf{p} = [p_2 \quad p_3 \quad p_4 \quad p_5 \quad p_6 \quad p_7 \quad p_8 \quad p_9 \quad p_0]^T. \quad (\text{A18})$$

The superscript T is the transpose operator.

Opening and closing rates,  $k_{OC}$  and  $k_{CO}$  in Fig. S3 are given by

$$k_{CO} = k_F \exp(\Delta E / 2k_B T) \quad (\text{A19})$$

$$k_{OC} = k_F \exp(-\Delta E / 2k_B T), \quad (\text{A20})$$

and Ca-binding and unbinding rates,  $k_{Ca}^+$  and  $k_{Ca}^-$  by

$$k_{Ca}^+ = k_b C_{FA} \tag{A21}$$

$$k_{Ca}^- = k_b K_D, \tag{A22}$$

where  $k_b$  is calcium binding coefficient,  $C_{FA}$  is calcium concentration at binding site and  $K_D$  is calcium dissociation constant  $k_B$  is Boltzmann constant,  $T$  is the absolute temperature and  $k_F$  is the opening/closing rate constant. The term  $\Delta E$  represents the difference in the channel intrinsic energy between open and closed states that depends on the hair bundle displacement, gating swing, and the number of bound calcium ions as

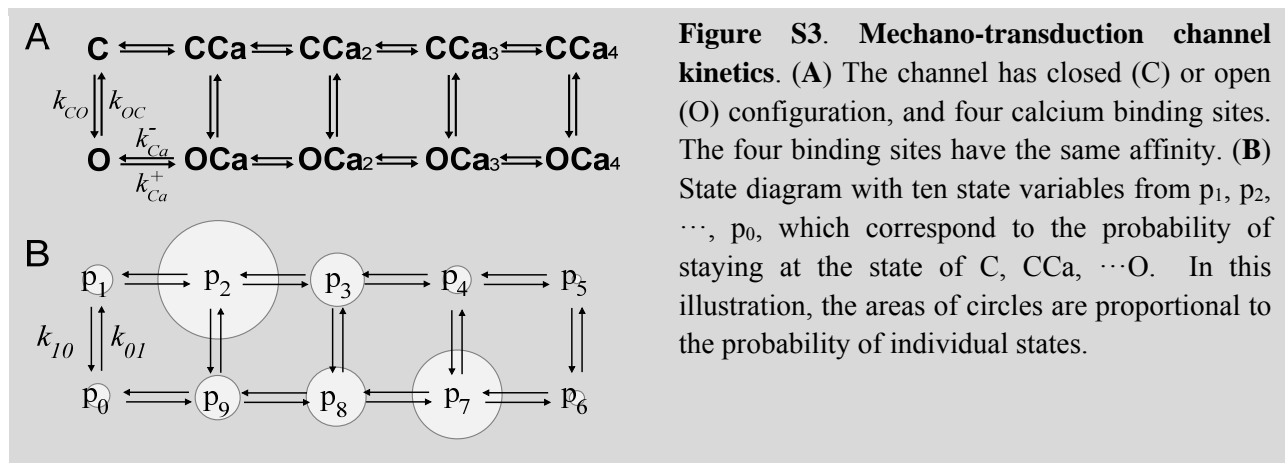
$$\Delta E = \gamma b k_G (X - X_S - n_{Ca} b_{fa}) \tag{A23}$$

where  $\gamma$  is the geometric gain,  $b$  is the gating swing,  $k_G$  is the gating spring stiffness,  $X$  is hair bundle displacement,  $n_{Ca}$  is number of bound calcium ions,  $b_{fa}$  is the coefficient to incorporate the effect of calcium-dependent adaptation and  $X_S$  is a constant used to set the resting open probability.

The equilibrium state ( $X_0, p_{00}$ ) is obtained by solving the system formed by taking Eq. A15 with left hand side set to zero, and Eq. 9 with stereocilia tip velocity and hydrodynamic force both set to zero

$$\left. \begin{aligned} \mathbf{A}_0 \mathbf{p}_0 + \mathbf{B}_0 &= 0 \\ k_{HB} X_0 - N k_G \gamma b p_{00} &= 0 \end{aligned} \right\} \tag{A24}$$

where, the subscript 0 denotes the parameter is evaluated at equilibrium.



Now, the Eq. 7 can be linearized about the equilibrium position by taking Taylor expansion of matrix  $\mathbf{A}$  and vector  $\mathbf{B}$ .

$$\mathbf{A} = \mathbf{A}_0 + \mathbf{A}'_0 (X - X_0), \quad (\text{A25})$$

$$\mathbf{B} = \mathbf{B}_0 + \mathbf{B}'_0 (X - X_0). \quad (\text{A26})$$

Substituting last two equations in the Eq. 7 gives linearized equation of the channel kinetics

$$\frac{d\mathbf{p}}{dt} = \mathbf{A}_0 + \mathbf{A}'_0 (X - X_0)\mathbf{p} + \mathbf{B}_0 + \mathbf{B}'_0 (X - X_0). \quad (\text{A27})$$

By assuming small perturbations around the equilibrium point in the form of time harmonic variations

$$X = X_0 + \delta X \exp(i\omega t), \quad (\text{A28})$$

$$\mathbf{p} = \mathbf{p}_0 + \delta \mathbf{p} \exp(i\omega t), \quad (\text{A29})$$

and substituting in the Eq. A27 to obtain

$$i\omega \delta \mathbf{p} \exp(i\omega t) = (\mathbf{A}_0 + \mathbf{A}'_0 \delta X \exp(i\omega t))(\mathbf{p}_0 + \delta \mathbf{p} \exp(i\omega t)) + \mathbf{B}_0 + \mathbf{B}'_0 \delta X \exp(i\omega t). \quad (\text{A30})$$

By using the first equation of the system Eq. A24 and neglecting higher order terms, we can solve for  $\delta \mathbf{p}$ .

$$\delta \mathbf{p} = (i\omega \mathbf{I} - \mathbf{A}_0)^{-1} (\mathbf{A}'_0 \mathbf{p}_0 + \mathbf{B}'_0) \delta X. \quad (\text{A31})$$

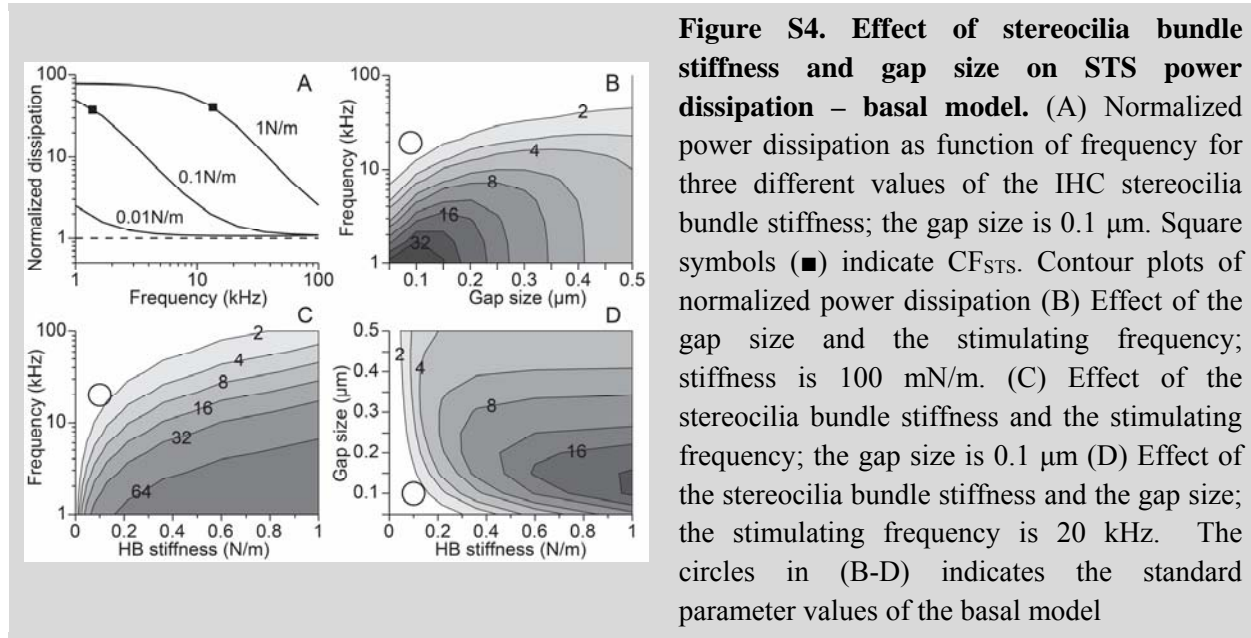


**Table S1. Model parameters**

Parameter	Value (short, tall)	Parameter description	Ref.
L ( $\mu\text{m}$ )	40	Length of the STS model	(3)
h ( $\mu\text{m}$ )	2, 5	Height of stereocilia bundle	(4-6)
gap ( $\mu\text{m}$ )	0.05 – 1.25	gap distance (see Fig. 1)	
$k_{\text{HB}}$ (mN/m)	100, 10	Stiffness of the stereocilia bundle	(7, 8)
$c_{\text{HB}}$ (nN·s/m)	10	Damping coefficient of the stereocilia bundle	
$k_{\text{G}}$ (mN/m)	3	Gating spring stiffness	(9)
b (nm)	2.0 – 2.9	Gating swing	(9)
$\gamma$	0.3, 0.1	Geometric factor	(9)
N	150, 100	Number of channels	(9)
$k_{\text{F}}$ ( $\text{s}^{-1}$ )	200, 50	Opening/closing rate	(9)
$k_{\text{b}}$ ( $\text{ms}^{-1}\mu\text{M}^{-1}$ )	0.4	$\text{Ca}^{2+}$ binding coefficient	(9)
$C_{\text{FA}}$ ( $\mu\text{M}$ )	1, 1 / 100, 50	$[\text{Ca}^{2+}]$ at the binding site (closed / open)	(9)
$K_{\text{D}}$ ( $\mu\text{M}$ )	100, 50 / 1, 1	$\text{Ca}^{2+}$ dissociation constant (closed / open)	(9)
$b_{\text{fa}}$ (nm)	1, 0.45	Gating swing	(9)
$\rho$ ( $\text{kg}/\text{m}^3$ )	1000	Water density	
$\mu$ (mPa·s)	0.72	Dynamic viscosity of the water	

## References

1. Harlow, F. H., and J. E. Welch. 1965. Numerical calculation of time-dependent viscous incompressible flow of fluid with free surface. *Phys Fluids* **8**:2182-&.
2. Freeman, D. M., and T. F. Weiss. 1988. The role of fluid inertia in mechanical stimulation of hair cells. *Hear Res* **35**:201-207.
3. Edge, R. M., B. N. Evans, M. Pearce, C. P. Richter, X. Hu, and P. Dallos. 1998. Morphology of the unfixed cochlea. *Hear Res* **124**:1-16.
4. Lim, D. J. 1980. Cochlear anatomy related to cochlear micromechanics. A review. *J Acoust Soc Am* **67**:1686-1695.
5. Furness, D. N., S. Mahendrasingam, M. Ohashi, R. Fettiplace, and C. M. Hackney. 2008. The dimensions and composition of stereociliary rootlets in mammalian cochlear hair cells: Comparison between high- and low-frequency cells and evidence for a connection to the lateral membrane. *J Neurosci* **28**:6342-6353.
6. Yarin, Y. M., A. N. Lukashkin, A. A. Poznyakovskiy, H. Meissner, M. Fleischer, J. Baumgart, C. Richter, E. Kuhlisch, and T. Zahnert. 2013. Tonotopic morphometry of the lamina reticularis of the guinea pig cochlea with associated microstructures and related mechanical implications. *J Assoc Res Otolaryngol*.
7. Beurg, M., J. H. Nam, A. Crawford, and R. Fettiplace. 2008. The actions of calcium on hair bundle mechanics in mammalian cochlear hair cells. *Biophys J* **94**:2639-2653.
8. Russell, I. J., M. Kossel, and G. P. Richardson. 1992. Nonlinear mechanical responses of mouse cochlear hair bundles. *Proc Biol Sci* **250**:217-227.
9. Nam, J. H., and R. Fettiplace. 2008. Theoretical conditions for high-frequency hair bundle oscillations in auditory hair cells. *Biophys J* **95**:4948-4962.